Aquacultural Engineering 107 (2024) 102476

Contents lists available at ScienceDirect

Aquacultural Engineering

journal homepage: www.elsevier.com/locate/aque

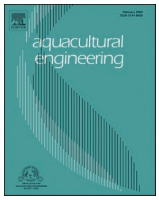

Design considerations for a continuous mussel farm in New England Offshore waters. Part I: Development of environmental conditions for engineering design☆

Richards C. Sunny [a,*], David W. Fredriksson [b], Igor Tsukrov [b], Longhuan Zhu [b], Matthew Bowden [c], Michael Chambers [b], Bill Silkes [d]

[a] A.I.S., Inc., in support of NOAA Fisheries, Northeast Fisheries Science Center, Milford Laboratory, 212 Rogers Avenue, Milford, CT 06460, United States
[b] The University of New Hampshire, 105 Main St, Durham, NH 03824, United States
[c] NOAA Fisheries, Northeast Fisheries Science Center, Milford Laboratory, 212 Rogers Avenue, Milford, CT 06460, United States
[d] American Mussel Harvesters, Inc., 165 Tidal Dr, North Kingstown, RI 02852, United States

ARTICLE INFO

Keywords:
Offshore aquaculture
Waves
Currents
Extreme value analysis
Return period
Joint probability distribution

ABSTRACT

Sustainable aquaculture in nearshore waters faces challenges such as stakeholder conflicts, environmental pollution, and spatial constraints. Offshore aquaculture offers a promising solution but requires robust engineering design to withstand extreme weather conditions. This study develops the environmental conditions essential for engineering the design of a continuous mussel dropper system in New England offshore waters. A potential farm location was identified using criteria including water depth, federal boundaries, seafloor suitability, farm size, and proximity to ports, based on bathymetric and sedimentary maps. Historical data from five wave monitoring stations and two current velocity stations were analyzed to model extreme environmental conditions, as waves and currents pose primary threats. The extreme wave and current conditions are modeled using the Weibull distribution, on the annual maximum hourly significant wave height data and the largest 0.3 % of current speeds. A newly proposed method combining Spalding's wall function with a fourth-order polynomial is used to enhance the current profile analysis. Additionally, a joint probability density function was developed for wave height and current velocity at a specific depth, providing insights into wave height, period, and wavelength for various return periods such as 10, 25, 50, and 100 years. The results suggest a 10-yr wave of 8 m significant wave height and a current speed of 1.68 m/s, while a 50-yr values are 9.4 m and 1.96 m/s respectively. These findings offer critical data on extreme wave and current conditions in New England's offshore waters, providing practical guidance for the engineering design of offshore mussel farms. This research advances offshore mussel farming and benefits the development of all types of offshore aquaculture systems.

1. Introduction

The offshore environment, characterized by its vastness and dynamic nature, has emerged as a critical arena for engineering innovation, particularly in the context of offshore aquaculture. This growing field, driven by the ever-increasing global demand for seafood, seeks to harness the potential of the open ocean for sustainable food production. In contrast to traditional coastal aquaculture, which grapples with spatial constraints and environmental challenges, offshore aquaculture endeavors to utilize the expansive and pristine waters of the open ocean to its advantage (Troell et al., 2014).

However, the offshore frontier poses a unique set of challenges, primarily rooted in the extreme environmental conditions that govern its waters. Unlike land-based aquaculture systems, the offshore environment is characterized by perpetual variability and extreme weather conditions. Among the myriad environmental variables, waves and ocean currents stand out as dominant forces that exert substantial loads on aquaculture structures. Consequently, the precise quantification of these waves and current dynamics, particularly during extreme events, becomes paramount for the safe, efficient, and sustainable design,

☆ This document is the result of the research project funded by the National Marine Fisheries Service, Office of Aquaculture.
* Corresponding author.
E-mail addresses: richards.sunny@noaa.gov (R.C. Sunny), David.Fredriksson@unh.edu (D.W. Fredriksson), Igor.Tsukrov@unh.edu (I. Tsukrov), longhuan.zhu@unh.edu (L. Zhu).

https://doi.org/10.1016/j.aquaeng.2024.102476
Received 13 May 2024; Received in revised form 9 October 2024; Accepted 13 October 2024
Available online 18 October 2024

Fig. 1. Geographical region of interest and federal water zone of New England waters. Federal waters is shown in darker blue color. The domain defined by the latitudes, 42˚ and 44˚, and longitudes − 71. 3˚ and − 69. 7˚.

construction, and operation of offshore aquaculture systems.

While traditional mussel farming predominantly occurs in inshore locations due to lower financial and technical requirements (Landmann et al., 2019), the limitations of inshore farming, including nutrient deficiencies, accumulation of mussel pseudofaeces, marine litter concerns (Lloyd, 2003), and navigational issues for marine vessels (Cole, 2002), have prompted a shift toward offshore aquaculture. Offshore farming offers financial benefits through increased productivity facilitated by high-quality water conditions and enhanced nutrition for mussels. However, the transition from nearshore to offshore aquaculture introduces significant environmental constraints, primarily in the form of high-energy waves and currents, necessitating a systematic engineering effort (Hall et al., 2018).

In this regard, the quantification of wave conditions is a critical endeavor. This involves a multifaceted approach encompassing wave measurement systems, statistical analyses, and numerical modeling techniques. Instruments such as buoys equipped with accelerometers and pressure sensors provide real-time wave data for offshore locations. Statistical tools, including probability distributions and Fourier transform analysis, extract vital wave characteristics such as significant wave height and period (Sobey, 1992). Spectral analysis techniques, exemplified by the Pierson-Moskowitz spectrum, help delineate the distribution of wave energy across different frequency components (Tayfun, 1980). Wave hindcasting and forecasting, supported by numerical wave models like SWAN and WAM, enable the representation of long-term wave climate statistics and short-term predictions (Hsu et al., 2005). Notably, the assessment of extreme wave statistics, as thoroughly explored by Goodman and Breslin (1976), is integral for designing offshore structures capable of withstanding a range of wave conditions.

Similarly, ocean currents, characterized by the directed flow of seawater, play a pivotal role in offshore aquaculture engineering. Currents influence structural stability, sediment transport, and nutrient dispersion, necessitating their precise quantification. Acoustic Doppler Current Profilers (ADCPs) are prominent instruments for measuring

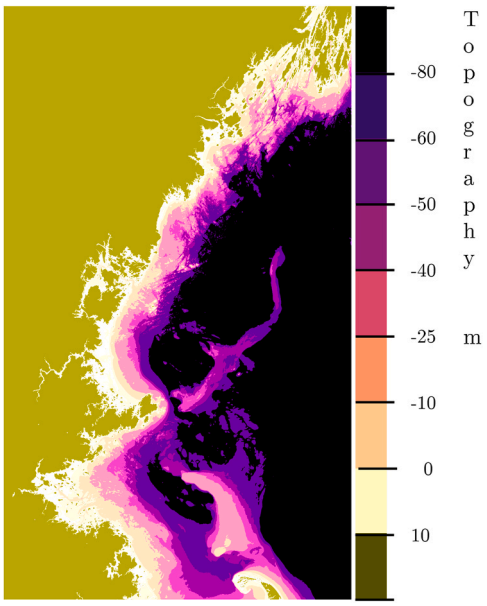

Fig. 2. Bathymetry map of the region of interest in New England water obtained from the Bathymetric Data Viewer by NOAA's National Centers for Environmental Information. The domain defined by the latitudes, 42˚ and 44˚, and longitudes − 71. 3˚ and − 69. 7˚.

water velocity profiles at various depths (Flagg and Kim, 1998). These devices emit acoustic signals, which bounce off particles in the water, allowing for the determination of current speed and direction. Numerical modeling, exemplified by the Regional Ocean Modeling System (ROMS) and the Princeton Ocean Model (POM), simulates ocean currents based on physical principles (Haidvogel et al., 2000; Blumberg and Mellor, 1987). Tidal analysis provides insights into tidal currents, crucial in coastal regions for navigation and infrastructure design (Cartwright and Edden, 1973). Moreover, analyzing current shear, which assesses variations in current speed with depth, is essential for understanding turbulence and its impact on submerged components. While tidal currents assume less significance in offshore regions, sediment transport analysis remains relevant for aquaculture projects, aiding in site selection and infrastructure design (Lynett, 2006). Additionally, data assimilation techniques enhance current predictions by integrating observational data into numerical models (Oke et al., 2015).

This paper, as part of a comprehensive two-part study, addresses the vital task of quantifying extreme environmental conditions in the offshore waters of New England. This endeavor lays the groundwork for a rigorous numerical modeling approach in Part II - work under review, which aims to assess the performance of a continuous mussel dropper system designed for New England's offshore waters. In the context of this study, "offshore" refers to areas located beyond the 3 nautical mile state waters boundary for the Atlantic Ocean, situated within U.S. Federal waters.

The research commences by identifying a potential farm location within New England's offshore waters, guided by specific criteria including water depth, federal water jurisdiction, seafloor suitability for screw anchor piles (also known as helical anchors), a farm area of 1000 acres, and proximity to New England coastal ports. Bathymetric and sedimentary maps serve as valuable tools for selecting example locations from an engineering perspective.

Subsequently, the study delves into the modeling of extreme environmental conditions at the chosen farm location. Rather than directly approaching the farm location, the research first establishes a broad statistical model encompassing the entire New England offshore region. This broader statistical framework forms the basis for estimating extreme conditions at the specific farm location through interpolation techniques. Historical wave data from five strategically located monitoring stations in the New England region, along with current speed data from two stations, contribute to the statistical model. The emphasis on wave and current modeling is justified by their significant impact on the structural stability of offshore mussel farms.

Extreme wave conditions are modeled using the Weibull distribution and annual maximum data, while extreme current conditions are similarly modeled using the Weibull distribution and the largest 0.3 % data subset. The statistical model, in conjunction with the dispersion equation, allows for the characterization of key wave parameters, including wave height, wave period, and wavelength, for representative waves corresponding to 10, 25, 50, and 100-year return periods. A similar approach is employed for current speed modeling. However, due to limitations in historical data, additional hourly averaged data from two stations collected over a 45-day period in 2023 are incorporated for enhanced interpolation. The research introduces a novel analytical approach that combines Spalding's wall function with a fourth-order polynomial framework to achieve a more accurate analysis of current profiles. This refined current profile data serves as crucial input for the simulations in Part II.

The ultimate selection of wave and current conditions as input for numerical simulations is based on compliance with the Ultimate Limit State (ULS) criteria recommended by Norwegian aquaculture standards, ensuring the structural integrity of mussel farm components (Wieling, 2023).

To facilitate the risk assessment and design optimization of mussel farm components, a joint probability density function is developed, integrating two key variables: wave height and current speed at a specific depth, with an assumption of independence. This joint probability density function is slated for utilization in Part II paper to estimate the probability of failure for various mussel farm components.

In conclusion, this work quantifies extreme weather conditions in the Northeast region in the context of offshore aquaculture engineering. By examining the extreme wave and current conditions in New England offshore waters using analytical and numerical modeling approaches, this research provides useful information to future researchers to navigate the basic challenges of the offshore aquaculture industry in the New England region contributing to the sustainable growth of this vital industry.

2. Mussel farm location

A commercially successful offshore mussel farm design from New Zealand was adopted as a standard case for this research. For identifying potential locations in New England waters, the following constraints were used within the domain defined by the latitudes, 42˚ and 44˚, and longitudes − 71. 3˚ and − 69. 7˚.

- Water depth within 25 and 60 m.
- New England federal waters.
- Seafloor sediment type suitable for screw anchor piles.
- 1000 acre approximate farm area.
- Within 10 NM distance from coast and near the ports of Portland, ME, Portsmouth, NH, and Boston, MA.

Fig. 1 shows the geographic region of interest with the federal water region shown in darker blue color obtained from the Bathymetric Data Viewer by NOAA's National Centers for Environmental Information. The bathymetry map of this region obtained from the same source after processing using QGIS (Kurt Menke et al., 2016) software and is shown in Fig. 2.

The federal water and bathymetry maps were then georeferenced for input to Google Earth software (Gorelick et al., 2017) to find the locations that satisfy the depth constraints as shown in Fig. 3. The surface geology map developed by Grizzle et al. (2009) shown in Fig. 4 is

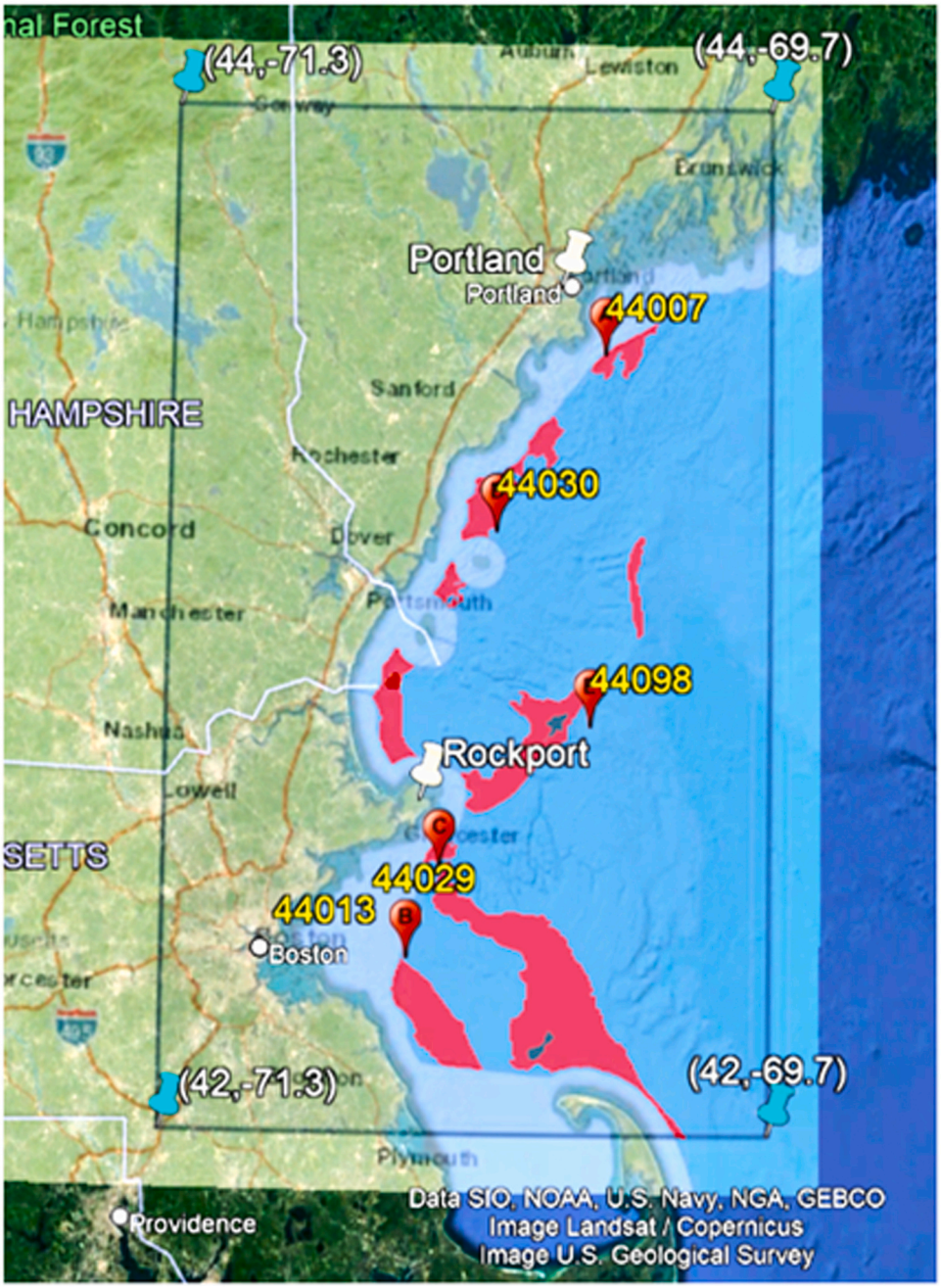

Fig. 3. Overlapped map of federal waters and bathymetry map of desired depth range 25–60 m. The lettered red markers show the locations of the five buoy stations: A (station 44007), B (station 44013), C (station 44029), D (station 44030), and E (station 44098). The domain is defined by the latitudes, 42˚ and 44˚, and longitudes − 71. 3˚ and − 69. 7˚. Zones satisfying constraints are shown in red color.

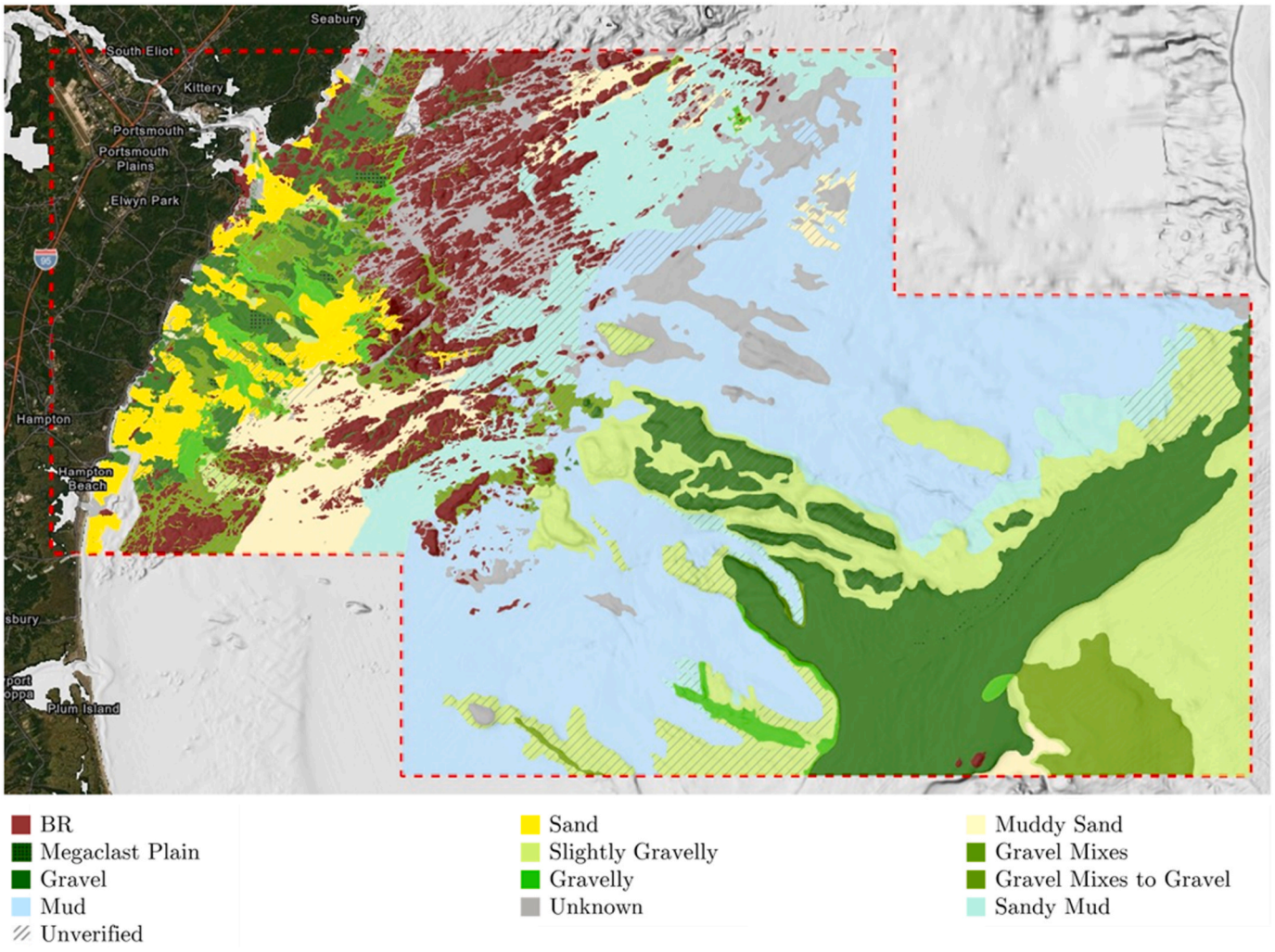

Fig. 4. The surface geology map developed by the University of New Hampshire used for determining potential locations for the mussel farm. The regions with the diagonal stripes mean unverified.

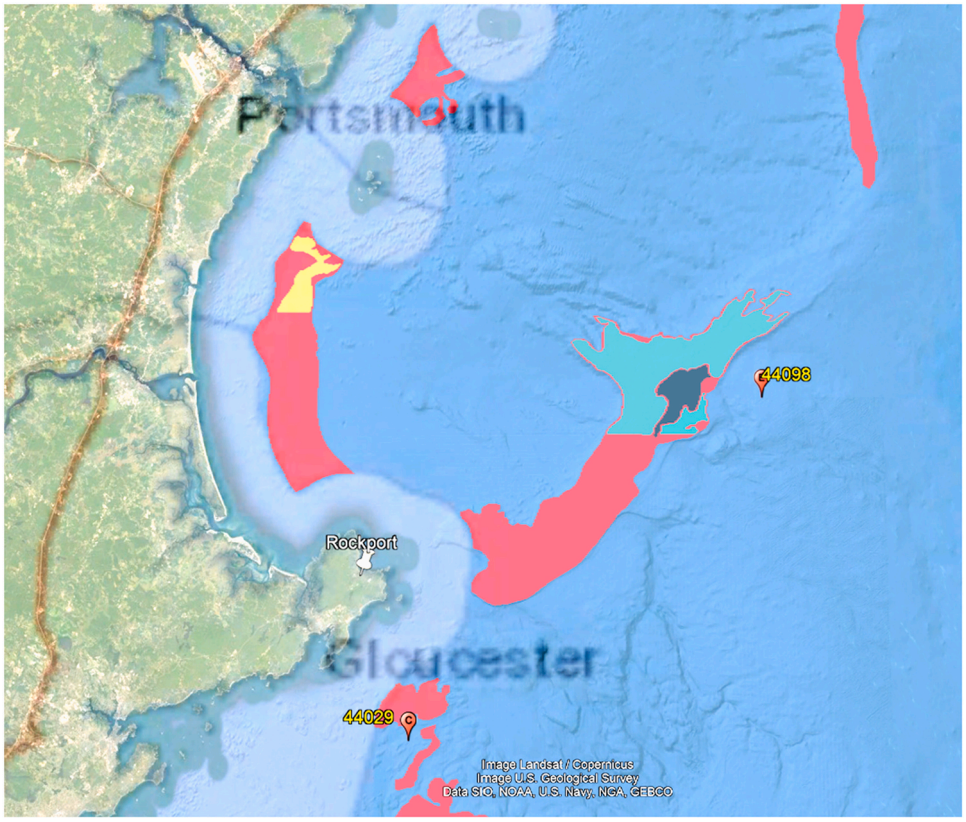

Fig. 5. Map showing the potential locations for the mussel farm that satisfies the federal water, water depth, and sea-surface geology constraints (in red). The yellow-colored zone represents sand and the green-colored zone, gravel. The red markers are the locations of buoy stations: C (station 44029), and E (station 44098).

Fig. 6. Selected location and design of a 1009 acre mussel farm with plot outlines, average wave, and current directions. Each plot (red rectangles) has a dimension of 360 m x 1100 m. 1000 ft navigation is provided between plots. Mussel lines (Yellow) are 190 ft apart and 6 plots of 100 Acres with 6 x 20 (120) mussel lines. The orange arrow represents the mean current direction, and the white arrow represents the mean wave direction.

Table 1
Locations of the five selected NOAA buoy stations in New England waters. Historical data from these stations are used for the statistical modeling of extreme weather conditions.

Station	Latitude	Longitude	Depth (m)	Coast (mi)
44013	42.346 N	70.651 W	64.6	10.0
44029	42.523 N	70.566 W	65.0	6.2
44098	42.800 N	70.171 W	80.0	23.8
44030	43.179 N	70.426 W	62.0	8.1
44007	43.525 N	70.140 W	49.0	4.2

provided as an overlay with the federal water and bathymetry map to obtain the potential location for the mussel farm as shown in Fig. 5. With this information, a set of potential sites were identified (Fig. 6) with the yellow-colored zone chosen for the mussel farm with the outline of the farm design. The major specifications of the mussel farm site are the following.

- 1009 Acre Farm Area (Green).
- Federal Waters.
- Sediment Type - Sand/muddy sand.
- Distance from the coast is 4.5 NM.
- 6 plots of 100 Acre with 6 × 20 (120) Mussel Lines.
- Each plot (red rectangles) has a dimension of 360 x 1100 m.
- Mussel longline length 1200 ft (360 m).
- Lines are 190 ft apart.
- 1000 ft navigation between plots.
- Nearest Weather Buoy Station IOSN3 - Isle of Shoals, NH.

3. Statistical modeling of environmental conditions

Extreme weather conditions pose a major threat to offshore aquaculture gear. Hence, the modeling of extreme weather events helps us to design for the probable critical events during the desired operational period. In this engineering design study, historical wave and current data from five NOAA buoys were obtained and return period statistics were developed. The historical dataset was collected by the National Data Buoy Center (NDBC) and it is published on their website. The location of the five selected buoys across the New England waters is shown in Fig. 3. Table 1 provides the location, water depth, and approximate distance to the coast of the selected buoys.

3.1. Extreme wave conditions

Station 44007 and 44013 have the longest historical data starting from 1983 and 1987, respectively. The instruments from station 44029 began collecting data in 2002, with those at station 44030 in 2003. Station 44098 has the least amount of historical data with information from 2009. The five NDBC buoys are still operating. The samples for modeling the extreme waves and currents were prepared using the annual maxima method. All the available data were used including those from stations with partial data during certain years. Significant wave height and dominant wave period data with one-hour intervals were used to model the extreme waves. In the annual maxima sampling method, the largest significant wave height (Hs) recorded in a calendar year and the corresponding dominant wave period (Tp) were considered. The annual maxima method is chosen so that each event is statistically distinct and it is a standard approach used in modeling extreme waves (Goda, 2010). In contrast with the total sample approach, the annual maxima method could have a limited data set. The "peaks over threshold method" should be avoided if the study is not to be done in a subjective manner. Statistical independence of data in time is assumed in modeling. The largest wave height recorded was 11.70 m in 2010 at station 44007. A significant wave height larger than 8 m is recorded 2, 6, 5, 7, and 5 times for stations 44007, 44013, 44029, 44030, and 44098. The significant wave height sampled data is shown in Fig. 7. For this study, the collected data is modeled using the Weibull distribution even though others can be applied based on "goodness of fit" criteria. The conditional form of Weibull distribution is

$$F(H_s \le \widehat{H_s}) = 1 - e^{-\left(\frac{\hat{H}_s - B}{A}\right)^k}, \quad (1)$$

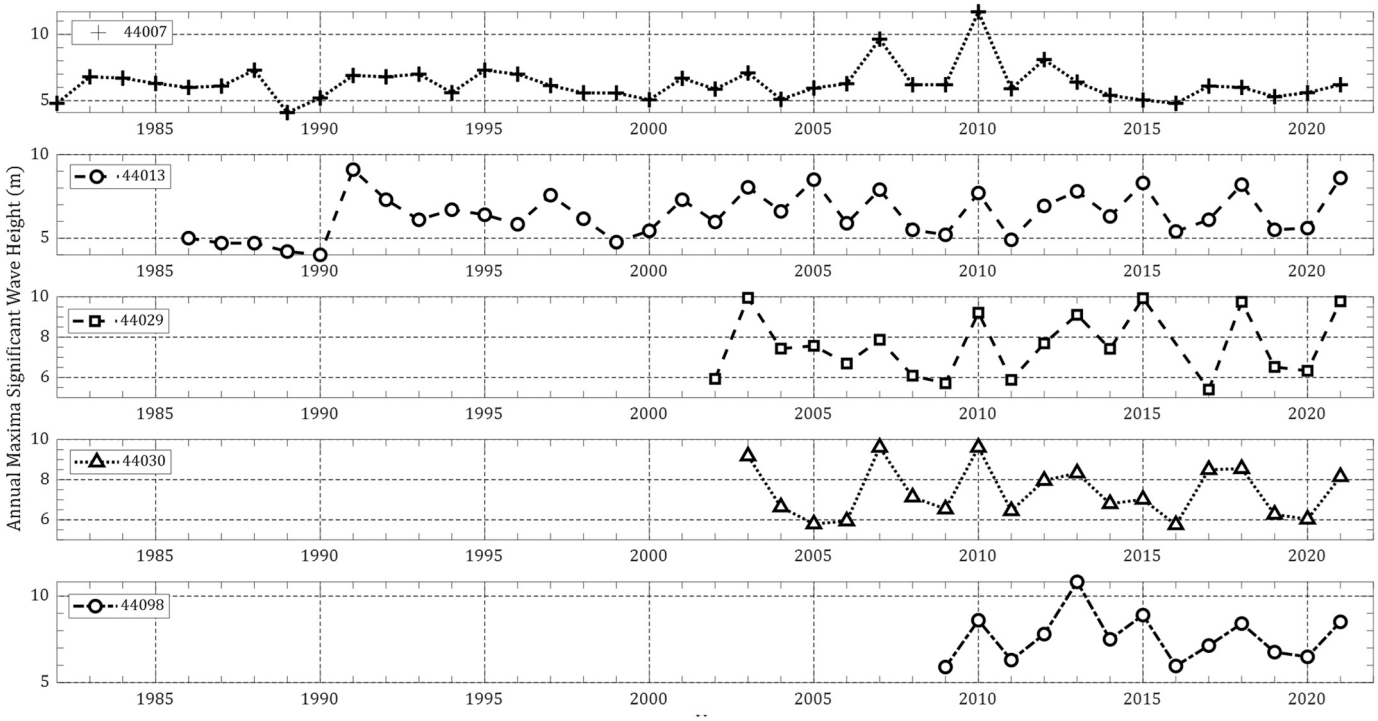

Fig. 7. Annual maxima historical significant wave height data from the five NOAA buoy stations. The location and other details about the stations are given in the Table 1.

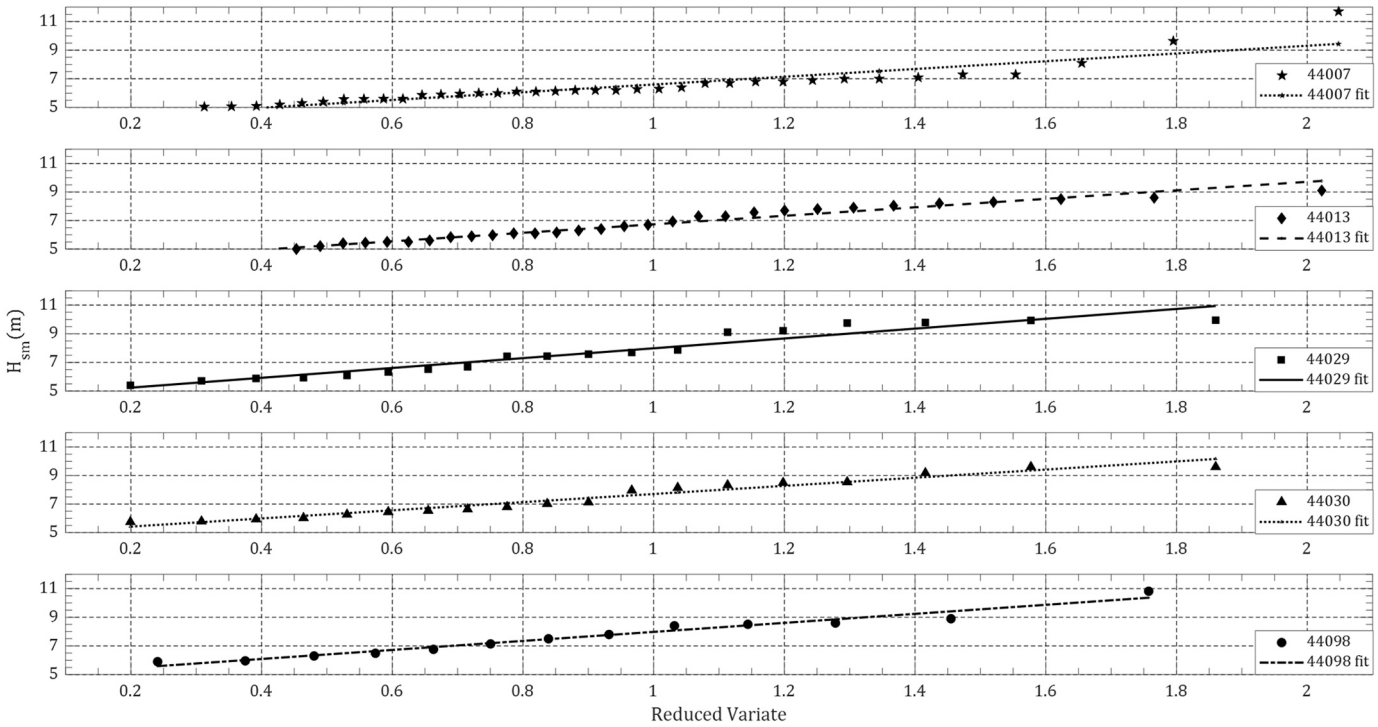

Fig. 8. Weibull distribution's reduced variate and least square fit for the extreme wave heights at the five NOAA buoy stations. The correlation between the reduced variate and the significant wave height is a measure of "goodness of fit", and all five stations have a correlation of 95 % or higher. The location and other details about the stations are given in the Table 1.

Table 2
Distribution Parameters of the best fit and the correlations of the fit.

Station	*A*	*B*	*k*	*r*
44007	1.954	4.5171	1.4	0.9509
44013	2.9787	3.7554	2.0	0.9880
44029	3.4337	4.5503	2.0	0.9657
44030	2.8576	4.8497	2.0	0.9788
44098	2.2416	5.5817	1.4	0.9846

where A, B, and k are the scale, location, and shape parameters, respectively. The parameter k is non-dimensional, but the parameters A and B have the same units as the random variable, i.e., the meter for the wave height. For k=1, the Weibull distribution would represent the exponential distribution and the distribution becomes broader as K gets smaller. For k =2, the Weibull distribution performs similarly to the lognormal distribution. The unbiased plotting position formula for Weibull distribution is

$$\widehat{F}_m = 1 - \frac{m - \left(0.20 + \frac{0.27}{\sqrt{k}}\right)}{N_T + \left(0.20 + \frac{0.23}{\sqrt{k}}\right)}, \tag{2}$$

where $m = 1, 2, \ldots, N$, k is the shape parameter, and N_T is the sample size. The reduced variate y_m for the m^{th} ordered data is calculated as

$$y_m = [-ln(1 - \widehat{F}_m)]^{\frac{1}{k}} \tag{3}$$

where $\widehat{F}_m$ is the nonexceedence probability. The parameters of the distribution, A and B in (4),

$$x_m = B + Ay_m \tag{4}$$

are then estimated using the least square fit method where x_m is the order statistics of extreme data in descending order. Since Weibull distributions have three parameters, the least-square fit is tested for four values of k; 0.75, 1.0, 1.4, and 2.0. The k value with the least error is chosen. Fig. 8 shows the reduced variate and the least square fit for the five NOAA station datasets. The correlation coefficients of the reduced variate fit are given in Table 2. It can be seen that the correlation is greater than 95 % as a "goodness of fit" for all five stations.

Fig. 9 shows the Weibull distributions for the significant wave height at the selected five NOAA stations obtained by substituting the parameter values for A, B, and k in (1). After finding the most probable Weibull distribution parameters for the observed data, the expected value for a given return period is estimated as

$$\widehat{x}_R = B + Ay_R \tag{5}$$

where the reduced variate y_R is a function of the return period R and the mean rate λ given by

$$y_R = [ln(\lambda R)]^{1/k} \tag{6}$$

The mean rate λ has a value of one when the annual maxima method is used. The extreme wave data has a large variability and it is likely that the estimated return values using the best-fitting Weibull distribution vary considerably around the true population. Techniques are provided by Goda (2010) to estimate the band for a given confidence interval(CI). For a 90 % CI, the true value is estimated using (7).

$$x_R = \widehat{x}_R \pm 1.645\sigma(\widehat{x}_R) \tag{7}$$

where $\sigma(\widehat{x}_R)$ is given by

$$\sigma(\widehat{x}_R) = \sigma_z.\sigma_x, \tag{8}$$

σ_z is the standard deviation of the reduced variate defined as

$$\sigma_z = \frac{[1.0 + a(y_R - c + \alpha \ln\nu)^2]^{1/2}}{\sqrt{N}}, \tag{9}$$

in which a is a constant, estimated as

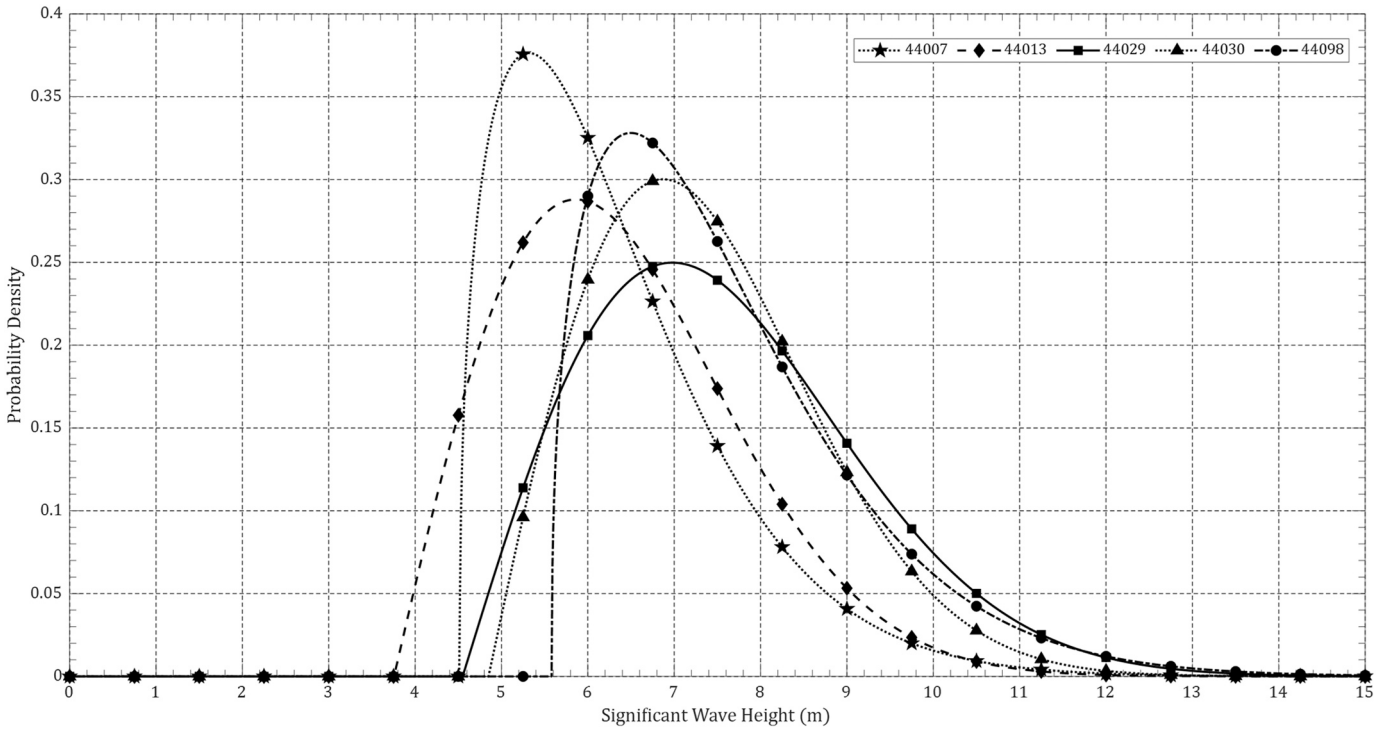

Fig. 9. Weibull probability density functions for the extreme wave heights at the five NOAA buoy stations. The location, depth, and distance from coast information about the stations are given in the Table 1.

Table 3
Constants for the standard deviation of return value for Weibull distribution (Goda, 2010).

k	a_1	a_2	κ	c	α
0.75	1.65	11.4	−0.63	0	1.15
1.0	1.92	11.4	0	0.3	0.90
1.4	2.05	11.4	0.69	0.4	0.72
2.0	2.24	11.4	1.34	0.5	0.54

$$a = a_1 e^{\left(a_2 N^{-1.3} + \kappa(-\ln\nu)^2\right)}, \tag{10}$$

In (10), ν is defined as the ratio of the number of data points to the number of extreme events, $\nu = \frac{N}{N_T}$, where N_T is the number of extreme events. The coefficients appearing in (9) and (10) have been estimated by (Goda, 2010) based on the Monte Carlo simulation studies and are provided in Table 3. The significant wave heights and corresponding return periods with the corresponding band with 90 % CI for the five NOAA stations are given in Fig. 10. The results are summarized in Table 4. According to this analysis, the 10-year expected return significant wave heights of the five stations range from 8.1 to 9.8 m with the largest one at station 44029 and the smallest at 44007. For the 50-year return period, the significant wave heights of the five stations range from 9.6 to 11.5 m, with the largest at station 44098 and the smallest at 44013, and for the 100-year return period, the significant wave heights of the five stations range from 10.1 to 12.3 m with the largest and smallest being recorded by the same as the 50-year return period. An analysis was conducted based on the depth and the significant wave heights for 10, 25, 50, and 100-year return significant wave heights showing a correlation. Fig. 11 shows this correlation with a linear least square fit with a 90 % confidence interval (CI). A positive correlation between the depth and significant wave heights is evident. The correlation is expected as the increase in depth typically means an increase in sea state roughness and the selected stations are expected to be impacted by the same extreme weather events such as Hurricanes or large-scale extratropical cyclones in the western North Atlantic Ocean (Northeaster) due to spatial closeness. The 10, 25, 50, and 100-year significant wave heights for the design depth are estimated based on the plots in Fig. 11. The most likely values corresponding to the design depth of 45 m are taken from the linear fit. The maximum and minimum values of the 10, 25, 50, and 100-year significant wave heights for the design depth are taken as the maximum of two values; 1. Maximum within the 90 % CI estimated from the relation between depth and wave height, and 2. Maximum significant wave height within the 90 % prediction interval for a station that is closest in terms of depth. For example, H_s Max for 10 years is taken as the maximum of 10.117 m (linear depth relation) and stations 44007's (depth = 49 m) 8.868 m from Table 4. Table 5 shows the estimated most likely, minimum, and maximum significant wave heights for return periods 10, 25, 50, and 100 years for the design depth of 45 m along with the correlation of the linear fit between the depth, and significant wave height in Fig. 11. The input wave heights for the numerical simulation for a return period T_R are finally picked for the corresponding depth based on Fig. 11. The fourth column in Table 5 gives the final input values for the significant wave height used in the numerical simulations. These values correspond to the most likely return values for 10–100-year return periods. The 90 % prediction interval of the system's response can be estimated by using H_s Min and H_s Max as the input loading conditions. The wave periods (T_p) corresponding to the annual maxima event are selected for finding the probability density function (PDF) of wave periods and the wave periods corresponding to the 10, 25, 50, and 100-year events estimated as

$$T_p = \alpha H_s^{\beta} \tag{11}$$

where α and β are found using the least square fit from the scatter plot of significant wave heights and peak wave periods (Goda, 2010). In Fig. 12, the significant wave period ($T_{1/3}$ or T_s) is considered as a function of T_p given by $T_s = T_p/1.1$ (Goda, 2010). For the numerical simulations, the fit for station 44007 is used as it has the closest water depth with a design depth of 45 m. So, the final significant wave heights and the significant wave periods corresponding to the 10, 25, 50, and 100 yr waves are

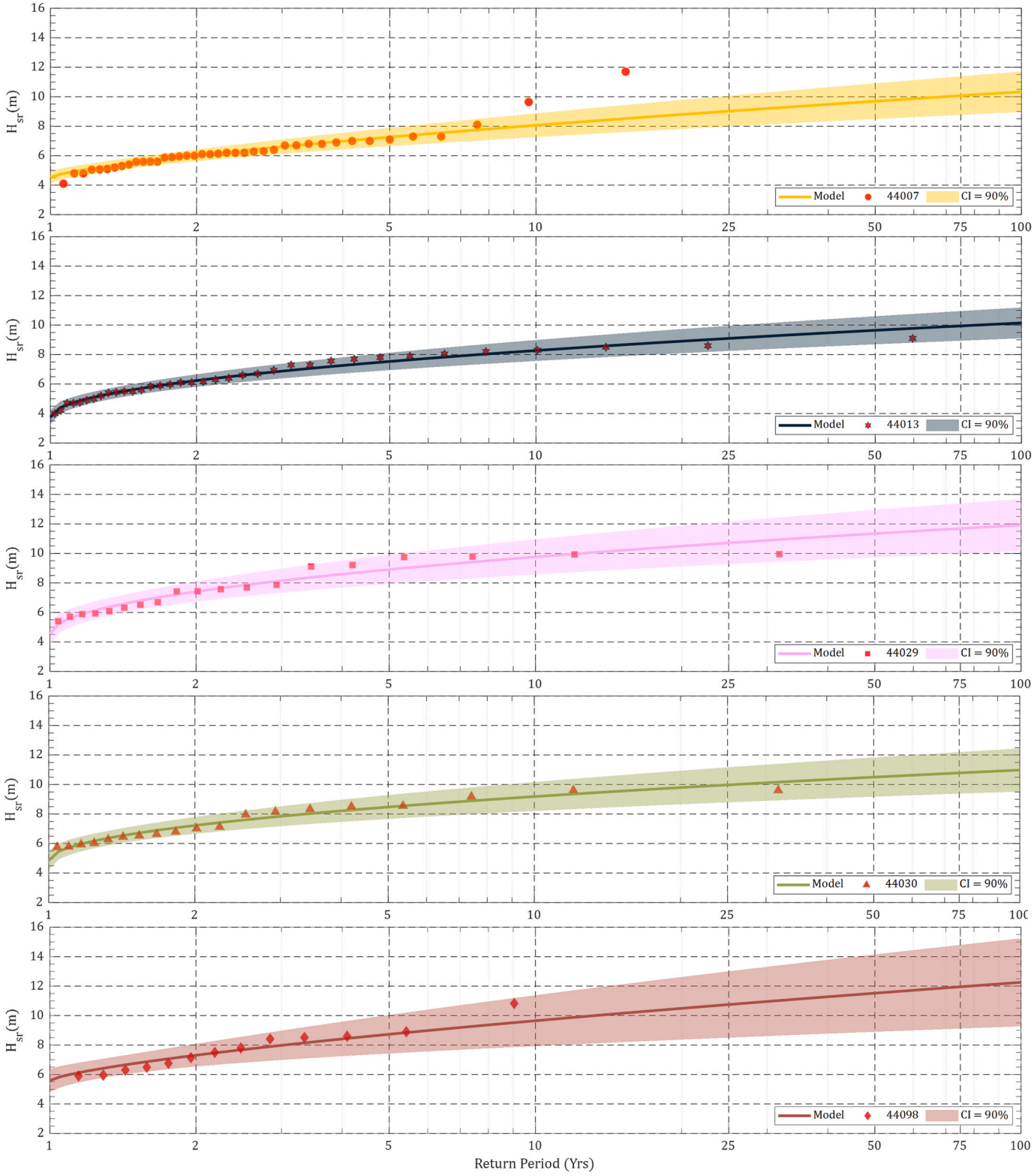

Fig. 10. Significant wave heights return period estimated using the Weibull distribution for the extreme wave heights at the five NOAA buoy stations. The location and other details about the stations are given in the Table 1.

Table 4
Estimated significant wave height (meters) return values and return periods with 90 % CI from the historical wave height data at the five selected stations.

Station	44007	44013	44029	44030	44098
10 yr	8.06	8.28	9.76	9.19	9.65
10 yr max	8.87	8.98	10.96	10.17	11.38
10 yr min	7.26	7.57	8.57	8.21	7.92
25 yr	9.02	9.10	10.71	9.98	10.75
25 yr max	10.06	9.95	12.16	11.16	13.00
25 yr min	7.98	8.25	9.27	8.79	8.50
50 yr	9.69	9.65	11.34	10.50	11.52
50 yr max	10.90	10.60	12.96	11.83	14.15
50 yr min	8.48	8.70	9.73	9.18	8.89
100 yr	10.33	10.15	11.92	10.98	12.25
100 yr max	11.71	11.19	13.69	12.44	15.24
100 yr min	8.96	9.10	10.14	9.52	9.27

provided in the Table 6. For numerical modeling with Hydro FE, the corresponding wavelengths were used. They were calculated from the implicit dispersion equation of linear wave theory (Dean and Dalrymple, 1995),

$$L = \frac{gT^2}{2\pi}\tanh\frac{2\pi h}{L}, \tag{12}$$

where T is the wave period, L is wavelength, and h is the water depth. Monochromatic waves, which are waves with the same wavelength are considered for this study, and the wave and current directions are either 0^o, 45^o, or 90^o with respect to the mooring line direction.

3.2. Extreme current conditions

Ocean current speed data is available from only two stations 44029 and 44030. The data set from station 44029 data includes years 2002–2022, and that from 44030 includes years 2003–2022. The annual maxima sampling method did not seem appropriate for ocean current speed modeling from the available data due to the outliers with magnitudes greater than even 20 times the standard deviation of the daily highs. The outliers are assumed to be of error and distribution quantiles were used to eliminate them. As the current speed varies with depth, to accurately model the environmental loading due to currents, it is necessary to capture the vertical current speed profile. For this purpose, all available historical data from the two stations at different depths were collected. Simple histograms with 50 bins of daily highs and daily average current speeds at three levels 2 m, 10 m, and 50 m from the water level are shown in Fig. 13.

The daily high current speeds at three depths were divided into quantiles and their respective mean values were used with piecewise linear fit as shown in Fig. 14. The standard deviations are provided to the right of the corresponding quantiles. One quantile that represents the extreme events in the best way is chosen to model the distribution and estimate the input values for the numerical model. The last three quantiles are (99.00^{th}–99.75^{th}), (99.00^{th}–99.90^{th}), (99.00^{th}–100^{th}). They represent extreme events. The large standard deviation associated with the quantile (99.00^{th}-100^{th}) denotes the presence of unrealistic outliers and hence the mean and standard deviation plot suggest the use of quantile (99.00^{th}–99.90^{th}) for modeling the distribution. The probability density functions (PDF) using Weibull distributions fitted for the three quantiles of extreme current speeds (99^{th} to 99.75^{th}), (99.00^{th}–99.90^{th}), (99.00^{th}–100^{th}) of daily highs are shown in Fig. 15. The PDF results also suggest the quantile (99.00^{th}–99.90^{th}) as it seems the best fit

Table 5
Correlation between depth and return values with 90 % CI from the historical wave height data at the design depth of 45 m. The return period (Return) is in years. Correlation is in percentage and the significant wave heights are in meters.

Return	Correlation	H_s Min	H_s	H_s Max
10	70.9	5.937	8.027	10.117
25	73.0	6.684	8.852	11.020
50	73.7	7.147	9.412	11.676
100	73.7	7.527	9.931	12.335

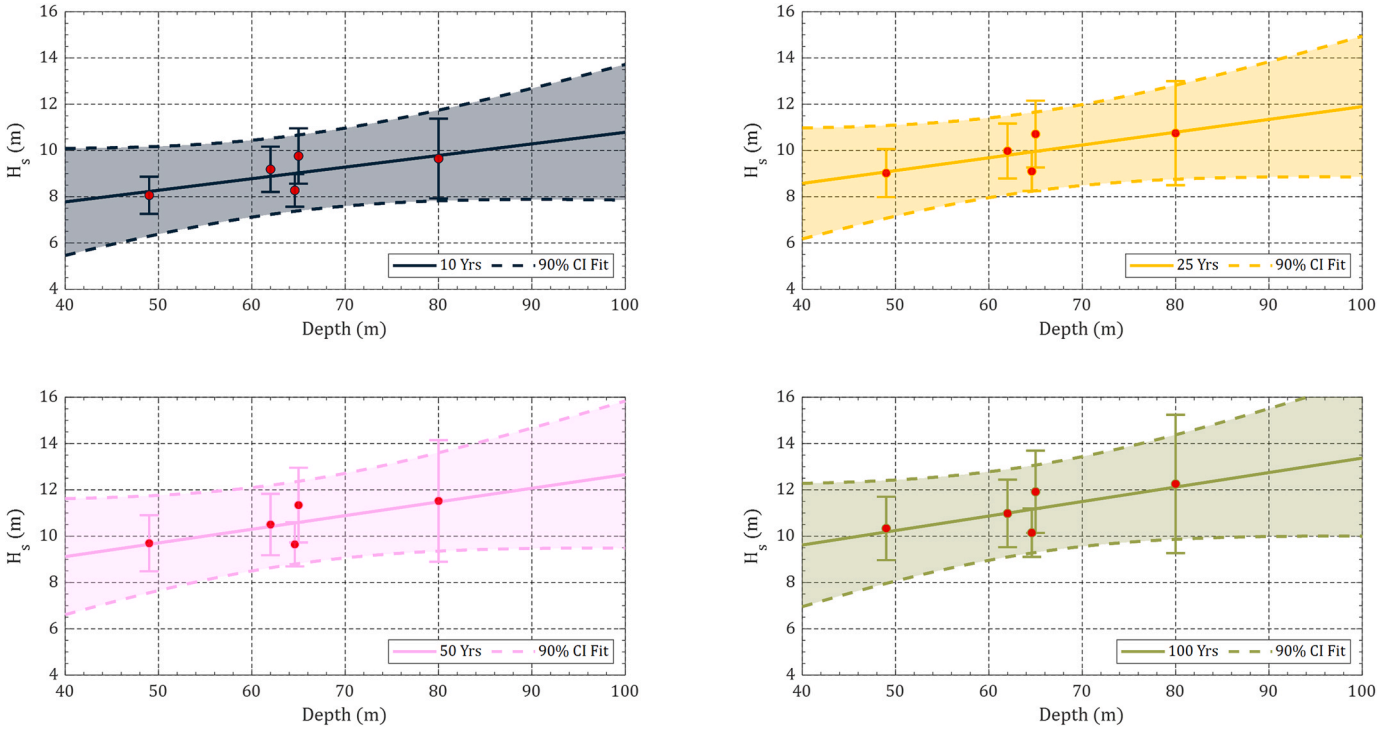

Fig. 11. Depth vs Significant wave heights for 10, 25, 50, and 100 year return period estimated using the Weibull distribution for the extreme wave heights at the five NOAA buoy stations. The location and other details about the stations are given in the Table 1.

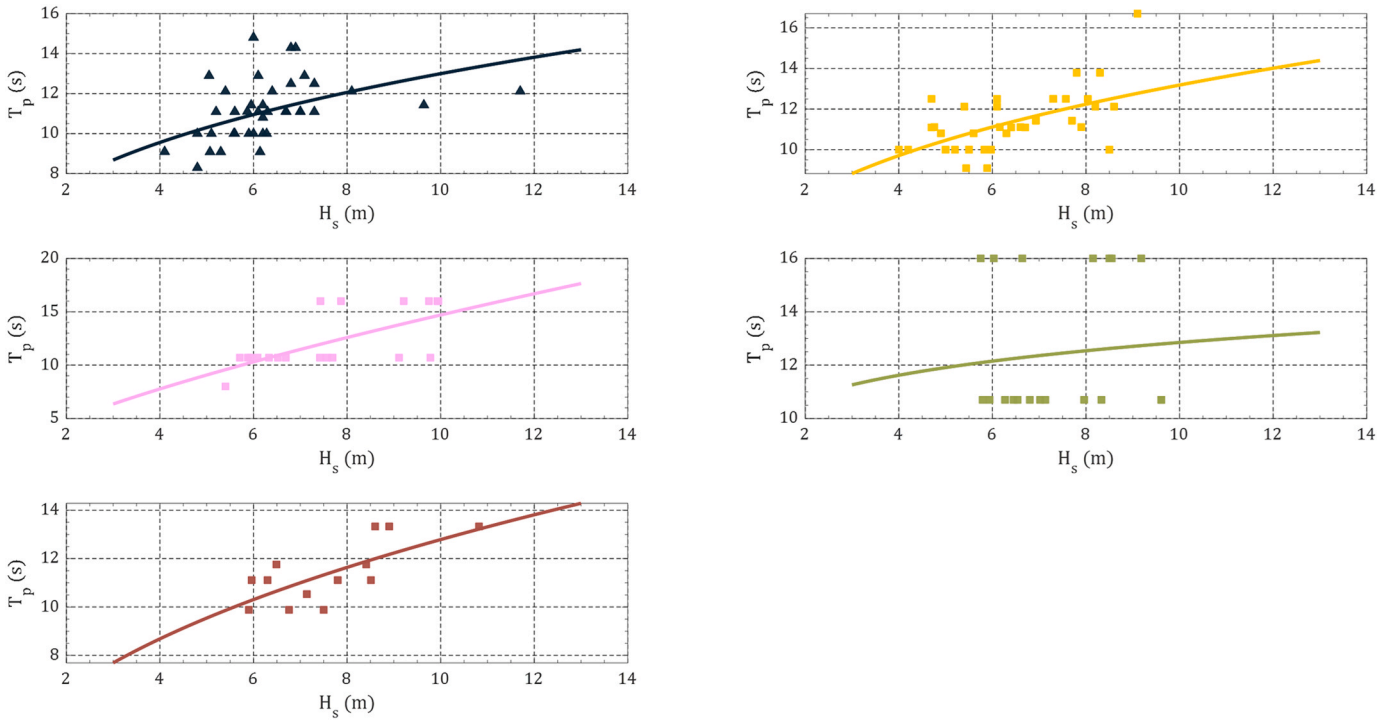

Fig. 12. Models fit from the scatter plot of significant wave heights and peak wave periods based on the equation $T_p = \alpha H_s^{\beta}$. 44007 (black), 44013(yellow), 44029 (pink), 44030 (green), 44098 (brown).

Table 6
Final significant wave heights, the significant wave periods, and the wavelengths corresponding to the 10, 25, 50, and 100 yr waves for the selected location with the design depth of 45 m.

Return Period	H_s(m)	T_s(s)	L(m)
10 yr	8.027	11.87	180.41
25 yr	8.852	12.21	188.55
50 yr	9.412	12.45	194.25
100 yr	9.931	12.63	198.52

qualitatively.

Finally, the relationship between the current speeds and the return periods was estimated using equations (1) to (3), and the results are shown in Fig. 16 and 17. The statistically predicted value for station 44030 at 50 m depth with 90 % CI seems unrealistic and the reason is unknown and can be suspected to be a measurement or calibration error or due to a physical phenomenon, currently not detected in the location such as internal waves. Because of this unrealistic nature, data from station 44030 is not used for the numerical simulations.

The decision to consider 99.00–99.75 % percentile data to model was based on the following analysis. Fig. 18 shows the correlation coefficient estimate for ranges starting from 99.00 % to 99.10–99.00–100 %. The intention is to include as much of the extreme data as possible while ensuring the fitted model accurately represents the data. The correlation coefficient is maximum for ranges ending at 99.9 % and it reduces largely past that. Hence the quantile (99.0–99.9) is suggested based on the correlation coefficient.

When the current speed is modeled using the data between the percentiles 99.0–99.9, the largest 0.1 percentile data is omitted. Even though the omitted data seems unrealistic it is very likely that they are larger than the rest 99.9 percentile data. In order to consider these larger data points, the location and scale parameter is extrapolated with the assumption that the shape parameter k is the same as that of the best fit for the quantile (99.0–99.9). The change of shape, scale, and location parameters for ranges starting from 99.00 % to 99.10–99.00–100 % for stations 44029 (left) and 44030 (right) are shown in Fig. 19. The estimation of scale and location parameters depends on the shape parameter. It can be noted that all three parameters start to vary before 99.20 % and after 99.75 % percentile for station 44029.

The shape parameter values for station 44029 for the quantile (99.0–99.9) at water depths 2 m, 10 m, and 50 m water depths are 1.4, 2, and 1.4 respectively. For station 44030 the shape parameters values are 2.0, 1.4, and 1.4 respectively. The variation of the scale and location parameter, as well as the standard deviation near the (99.0–99.9) quantile data using the above shape parameter values, are used to extrapolate the dataset to obtain the omitted largest 0.1 percentile data as shown in Fig. 20. A second-degree polynomial curve using the least square fit is used to extrapolate the location parameter, scale parameter, and standard deviation; its correlation coefficient is shown in Table 7. It can be seen that all the quadratic fits have a correlation larger than 99.3 % for station 44029, and 97 % for station 44030 except for the location parameter for station 44030 at 50 m depth which is around 90 %. These results also suggest an anomaly or error with the current speed observed at station 44030 at 50 m depth. The correlation for the scale parameter for station 44029 and the correlation for the standard deviation fit is higher than 99 %. The probability density functions for the two stations 44029 and 44030 at three water depths of 2 m, 10 m, and 50 m are shown in Fig. 21 Calculated return values of current speed using the extrapolated scale parameter, location parameter, and standard deviation for the two stations 44029 and 44030 at depths of 2 m, 10 m, and 50 m are shown in Fig. 22. Even though the data from station 44030 at 50 m depth seems acceptable from a statistical point of view, the predicted return values are above the realistic limit. The cause of this needs future investigations and for this reason, the fitted models for station 44030 are not used further in this research. The variation of using the fitted Weibull distribution, the 10, 25, 50, and 100-year current speeds at the two selected stations at three water depths are given in Table 8.

The environmental load conditions for the extreme events corresponding to the 10, 25, 50, and 100 yr return periods using the most likely scenario are provided in the Table 9

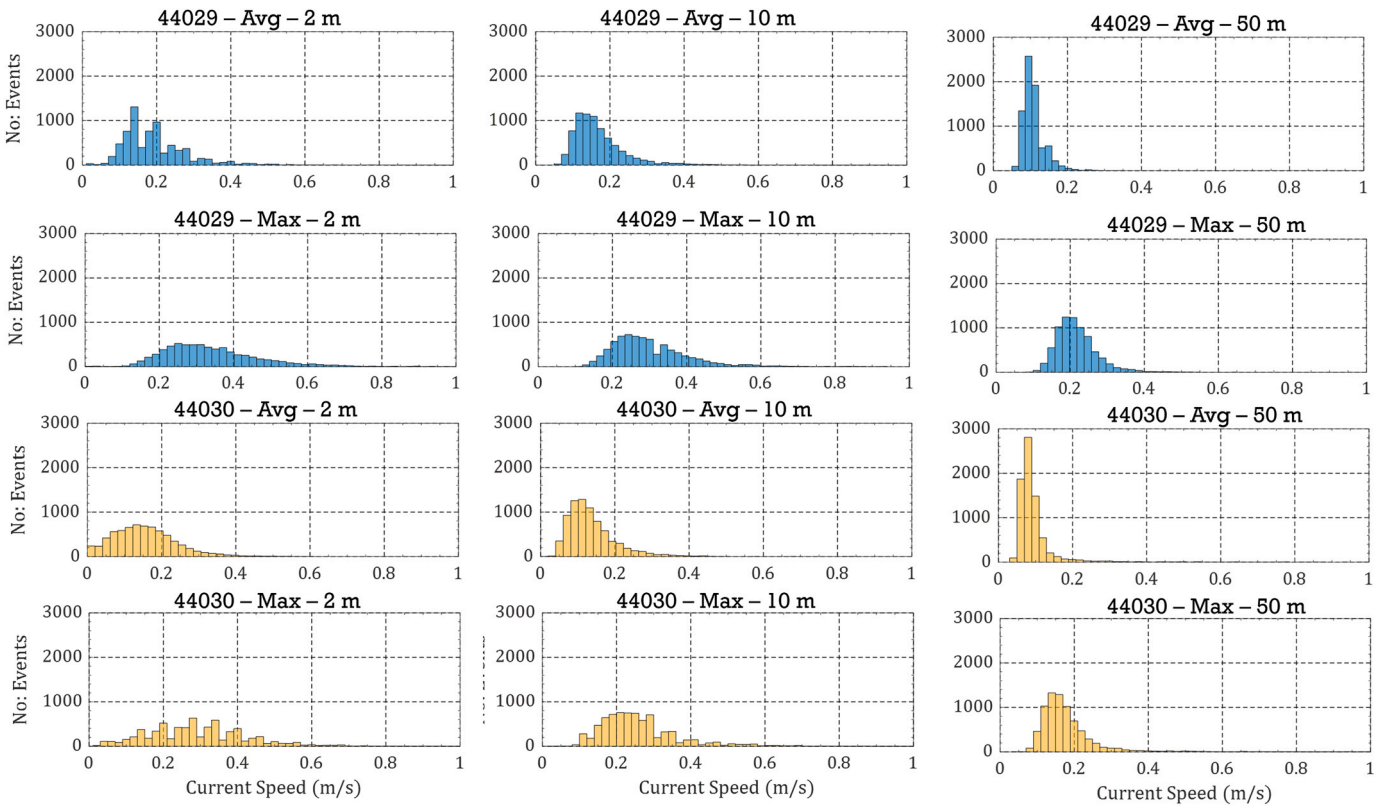

Fig. 13. Histograms of ocean current speeds at three depths (2 m, 10 m, and 50 m) of two stations 440029 (blue) and 440030 (yellow). For both locations, for both the average and the maximum when depth increases from 2 to 10–50 m, the distributions are getting more skewed and have lesser variance or more peaky while the maximum location shifts to the left, showing lower current speed with increasing depth. Station 44029 has a higher median current speed than 44030 at all depths for average and maximum cases. The average and maximum distribution at all three depths of both stations is very similar in shape, suggesting a good correlation. The daily maximum of both stations at all depths has a higher variance than the daily average cases and the peak locations shifted to the right as expected indicating higher median cuurent speed.

3.2.1. *Current speed profile*

An estimate of extreme loading conditions requires the vertical current speed profile. For this purpose, a model is to be fit using the estimated current speeds at the three points. The simplest model is the piecewise linear model which interpolates between the points of known current speeds. However, a piecewise linear model is continuous but not differentiable or smooth at nodes. Therefore a cubic polynomial fit is applied and it is differentiable or smooth everywhere. The four parameters of the curve can be solved using the three estimated current speeds and by the no-slip boundary condition at the sea floor. It should be noted that as a fitted dataset, the cubic polynomial does not represent a physical process The study of wall-bounded turbulent flow shows that in the viscous (laminar) sublayer, which is attached to the boundary surface, the mean velocity is expressed as

$$U^+ = \frac{U}{U*} = \frac{U}{\sqrt{\tau_w/\rho}} = y^+ = \frac{yU*}{\nu} \tag{13}$$

where U is the free stream velocity, U^* is the friction velocity, U^+ is the dimensionless velocity, y^+ is the dimensionless wall coordinate, τ_w is the wall shear stress, ρ is the fluid density, and ν is the kinematic viscosity of the fluid (Kadivar et al., 2021). This is applicable for $y^+ < 5$. The next region is called the log-layer and has the natural logarithmic velocity, referred usually as the law of the wall which is given by

$$U^+ = \frac{1}{\kappa}\ln(y^+) + C, \tag{14}$$

where κ is known as the von Karman constant which is approximately 0.41 and C is the roughness constant. This is valid for the region $y^+ > 30$. Spalding et al. (1961) proposed an approach that considers the viscous, buffer, log law, and defect layers of wall-bounded flow and has been validated with experimental data for a wide range of $0 \leq y^+ \leq 2000$. The Spalding law-of-the-wall is given by

$$y^+ = U^+ + e^{-\kappa C}\left(e^{\kappa U^+} - 1 - \kappa U^+ - \frac{(\kappa U^+)^2}{2} - \frac{(\kappa U^+)^3}{6}\right). \tag{15}$$

An investigation was then conducted to determine the best curve fit representation for the current speed profile (piecewise linear, cubic, Spalding's wall function). For this purpose, hourly current speed data for the 45 days at station 44029 was analyzed. Unlike the historical current speed data, which was available only at the three depths, this data consists of current speeds at 14 depths. Fig. 23 shows the average profile and statistics of the 45 days of data, while Fig. 28(Appendix A) shows the piecewise linearly fit quantile mean current profiles of 45 days of hourly averaged data at station 44029. Three sets of the current speed quantile profiles to represent the 45 days of data were created using the piecewise linear, cubic, and Spalding's wall functions and the data at the three depths which are available for the historical data; i.e. 2, 10, and 50 m. A new function named Spalding-Poly is proposed that combines Spalding's wall function and a fourth-order polynomial. This function has the same profile as that of Spalding's wall function for the largest 25 % of depth or near the wall. A fourth-order polynomial with five parameters defines the current speed profile starting from the surface to 75 % of water depth. At the transition point from Spalding's wall function to the polynomial function, three characteristics of the functions are matched; value, slope, and curvature. The polynomial function also matches the measured data value at the two locations near the surface. Thus a fourth set of profiles is created using the proposed function. The four sets of current speed quantile profiles are shown in Fig. 26(Appendix A). It can

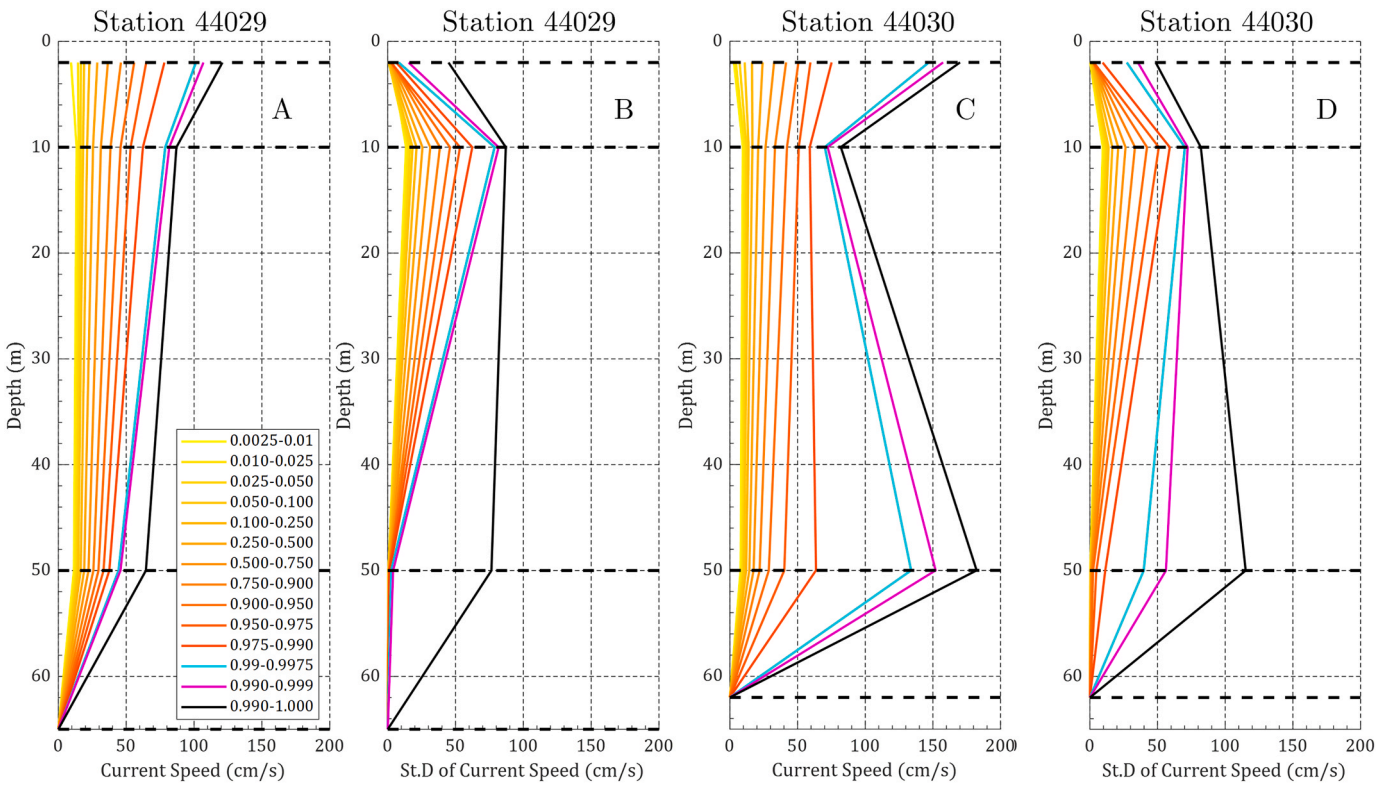

Fig. 14. Daily high current speeds at three depths divided into quantiles and the piecewise linear fit using their respective mean values. Columns A and B belong to station 44029, and C and D belong to station 44030. Columns B and D represent the quantiles of the standard deviation.

be seen that the cubic and piecewise linear functions have unrealistic profiles close to the seafloor and Spalding's wall function has poor performance near the surface. The newly proposed function seems to perform well. To quantify the performance, error plots were created by comparing the four sets of created profiles to the data at the 14 depths. This is shown in Fig. 27 (Appendix A). Quantitative error analysis shows that Spalding's wall function and the proposed function have the least error in the range of 45–65 m. Between depths 10–44 m, Spalding's wall function has the maximum error, followed by cubic and the proposed function. Piecewise linear function has the least error in this range. While considering the entire depth, the error is the least for the proposed function; Splading-Poly. Thus, it is used to model the extreme current speed profile for the design location.

From (15) and (13), it can be seen that the unknowns for creating a profile using Spalding's wall function $S(y)$ are U^* and C. C is the roughness coefficient and can be assumed to be constant for a location. Thus for creating the profiles for the 45 days of data from station 44029, C and U^* are solved numerically using the mean data from the 58 and 50 m water depths shown in Fig. 23. The value of C was found to be −35.756 and the shear stress to be 1.01 Pa. Now, since the function is implicit in U, numerical solutions via iterations are obtained for each depth level and thus the profile is obtained.

The proposed function, Spalding-Poly $P(y)$ has the same profile as Spalding's wall function for the largest 25 % of depth or near the wall which gives $P(y)_{0-0.25} = S(y)$. The five parameters are solved using the following known values; $P(y = y_{0.25})$, $P(y = 10)$, $P(y = 2)$, $P'(y = y_{0.25})$, and $P''(y = y_{0.25})$.

Final Current Speed Profiles for extreme current events: Final current profiles for extreme current events at the design depth are obtained by linear scaling along depth without change in the current speed magnitude using the newly proposed function. Results are shown in Fig. 24. Current profiles are created for return periods 10, 25, 50, and 100 years for the most likely, minimum, and maximum cases within the 90 % CI. The most likely profiles (the second column B in Fig. 24) are used as input to the numerical model. Minimum and Maximum value (columns A and C in Fig. 24) profiles can be used as loading inputs to the numerical model for estimating the system's responses within a 90 % prediction interval.

3.3. Joint probability density function for waves and currents

We suggest an approach to quantify the risk of structural failure of different components of the mussel farm so that the appropriate safety factors can be used by the farmers and suggested by the regulatory agencies.

A multivariate probability density function or a joint probability density function(PDF) based on the individual PDFs for the significant wave heights and the ocean current speed is used for this. The stationarity and independence of the variables are assumed for this basic analysis. The estimation of the probability of failure of the components is presented in part II which is under review. Joint PDF is a non-negative function f_{XY}: $R^2 \rightarrow R$, such that, for any set $A \in R^2$, we have

$$P[((X,Y) \in A] = \iint_A f_{XY}(x,y)dxdy, \tag{16}$$

where X and Y are the two random variables, P is the probability, and A is domain area. This means that for small positive δ with the independence assumption, we have

$$P(x - \frac{\delta_x}{2} < X \leq x + \frac{\delta_x}{2}, y - \frac{\delta_y}{2} < Y \leq y + \frac{\delta_y}{2}) \approx P(X)P(Y)\delta_x\delta_y. \tag{17}$$

Fig. 25, shows the estimated joint PDF combining the historical significant wave height and current speed data from station 44029.

4. Conclusion

This study provides a comprehensive analysis of extreme environmental conditions in New England's offshore waters, which is a critical

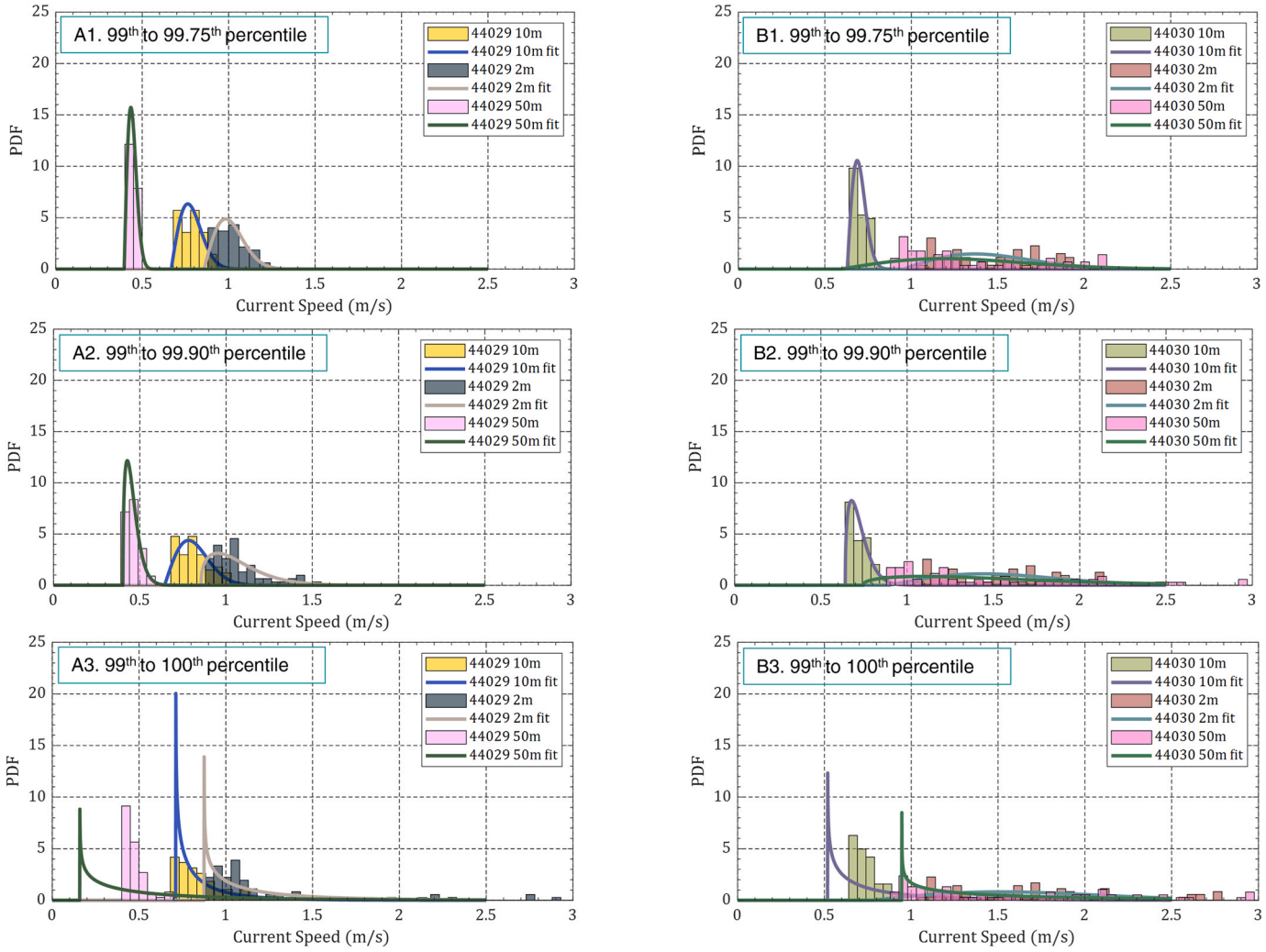

Fig. 15. Weibull probability density functions (PDF) for the three quantiles of extreme current speeds 1. 99^{th} to 99.75^{th}, 2. 99.00^{th}-99.90^{th}, 3. 99.00^{th}-100^{th} of daily highs for the past 20 years (01/01/2001–12/31/2022) at the two NOAA buoy stations, A. 44029 and B. 44030 at three water depths.

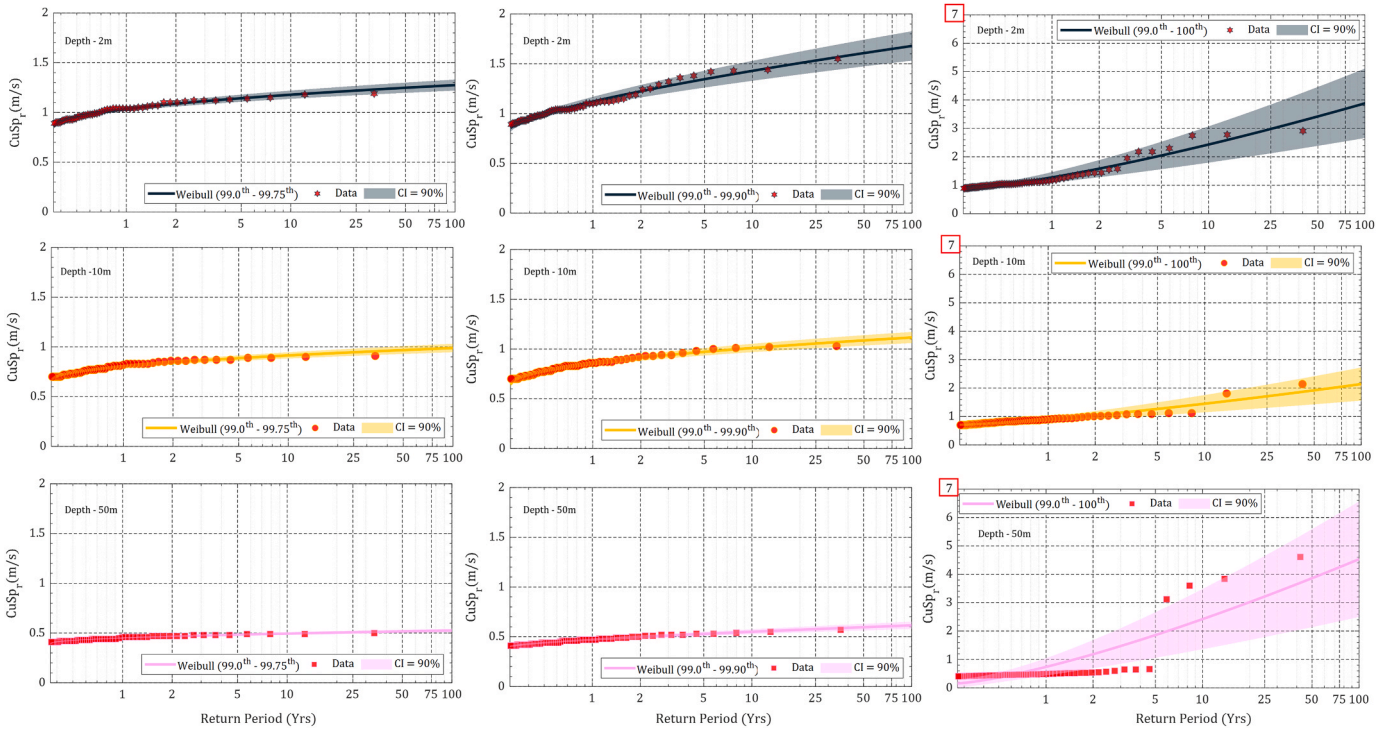

Fig. 16. Current speed vs return period estimated using the Weibull distribution for the three quantiles of extreme current speeds 99^{th} to 99.75^{th} (left column), 99.00^{th}-99.90^{th} (center column), 99.00^{th}-100^{th} (right column) of daily highs for the past 20 years at station 44029. Colors represent the depth: 2 m (gray), 10 m (yellow), 50 m (pink). The historical data are shown as points and fitted models as lines. The location and other details about the stations are given in the Table 1.

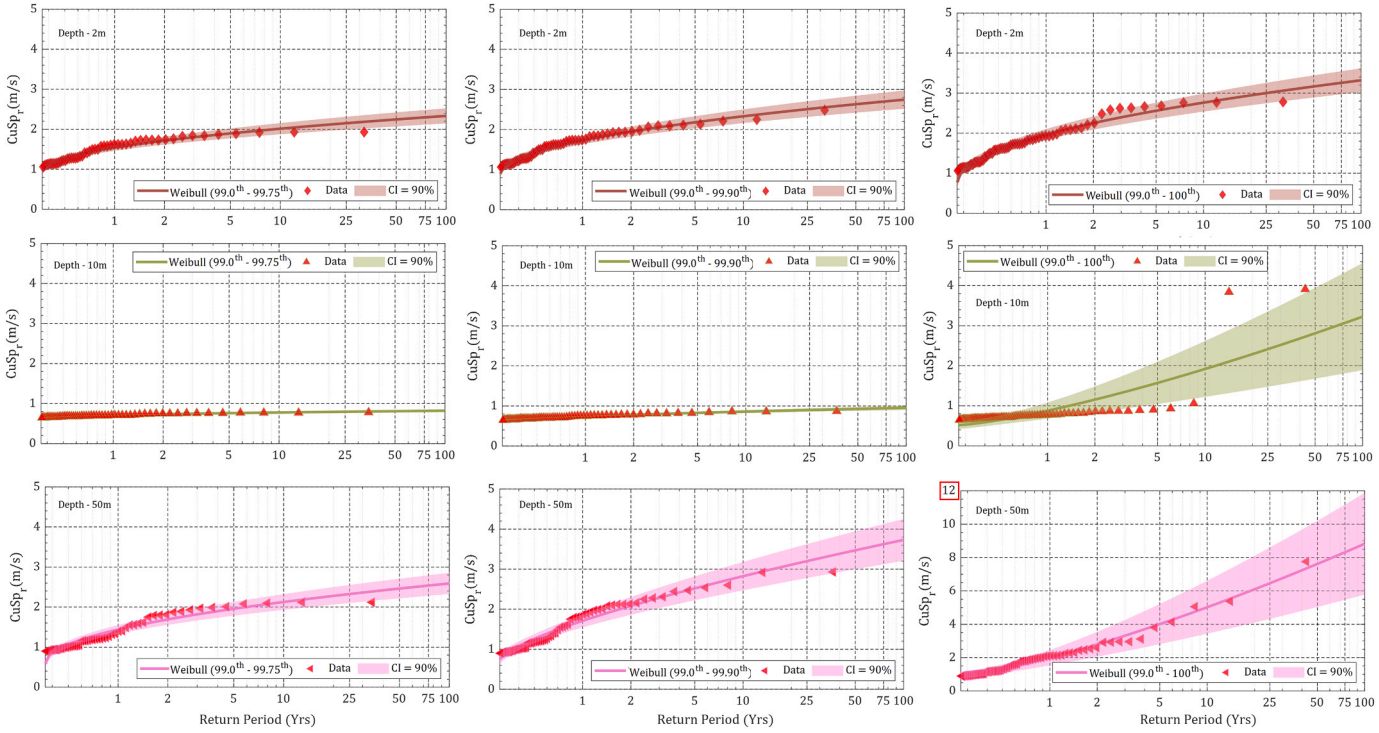

Fig. 17. Current speed vs return period estimated using the Weibull distribution for the three quantiles of extreme current speeds 99^{th} to 99.75^{th} (left column), 99.00^{th}-99.90^{th} (center column), 99.00^{th}-100^{th} (right column) of daily highs for the past 20 years at station 44030. Colors represent the depth: 2 m (gray), 10 m (yellow), 50 m (pink). The historical data are shown as points and fitted models as lines. The location and other details about the stations are given in the Table 1.

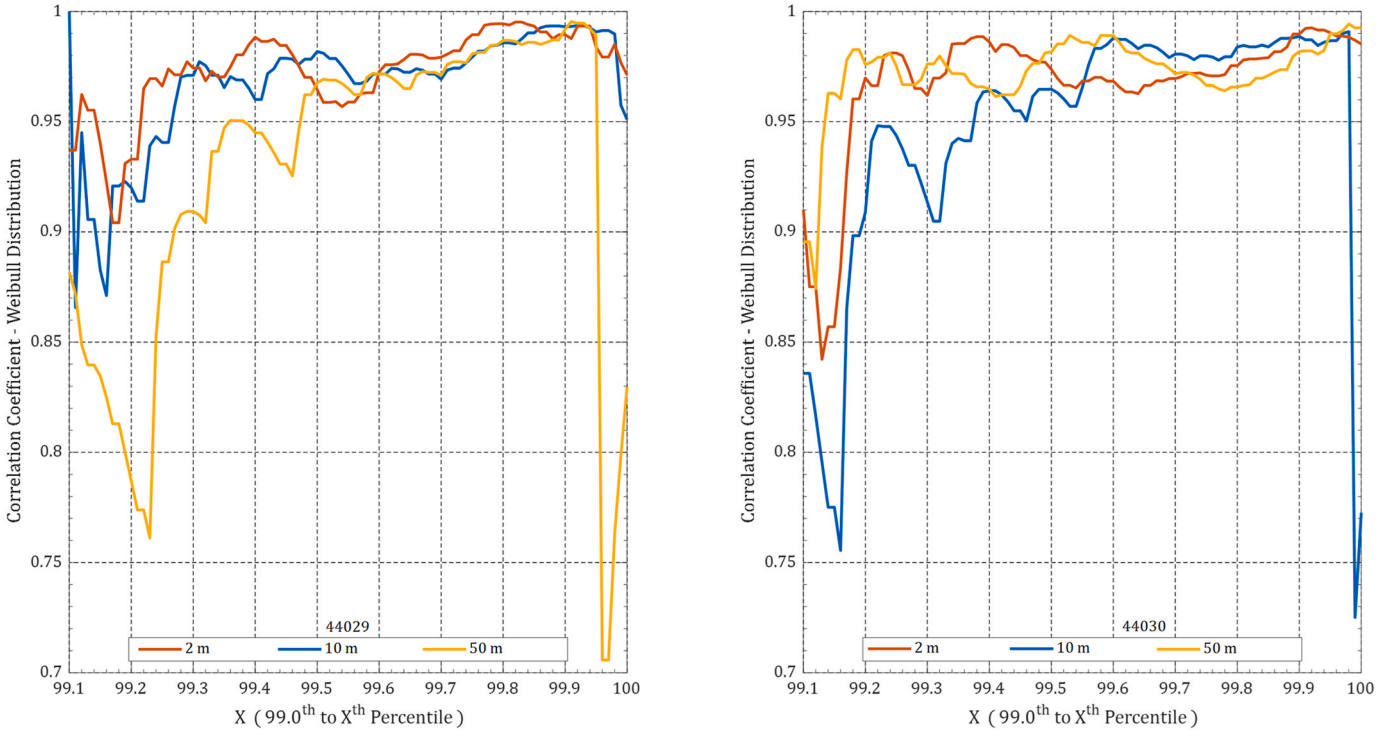

Fig. 18. Correlation coefficient estimate for ranges starting from 99.00 % to 99.10–99.00–100 % quantiles for stations 44029 (left) and 44030 (right) for the Weibull distribution model. The location and other details about the stations are given in the Table 1. It can be seen that the correlation coefficients are above 90 % from 99.3 percentile and increasing to about 98 % before drastically dropping for the (99.0–99.9) to (99.0–100) percentile data suggesting an improved model in this region.

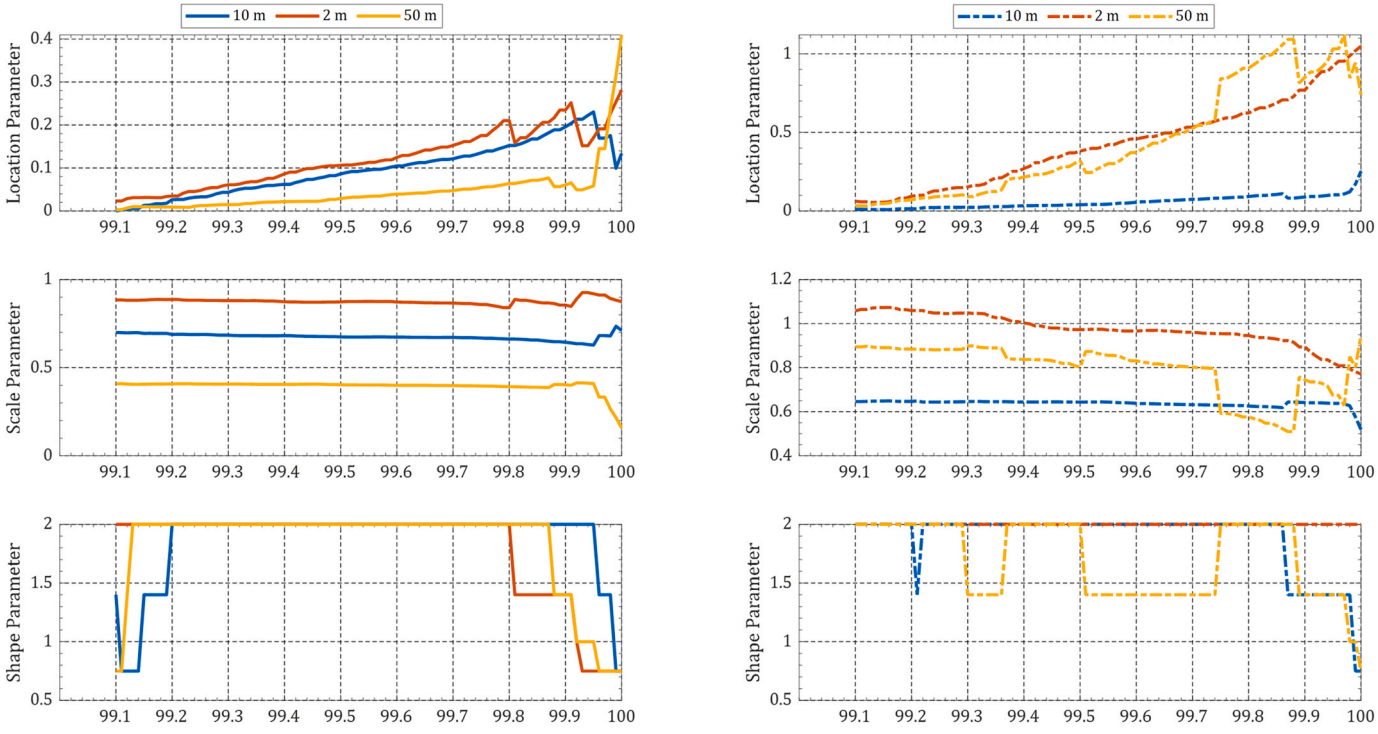

Fig. 19. The change of shape, scale, and location parameters for the Weibull distribution for ranges starting from 99.00 % to 99.10–99.00–100 % quantiles of current speeds for stations 44029 (left) and 44030 (right).

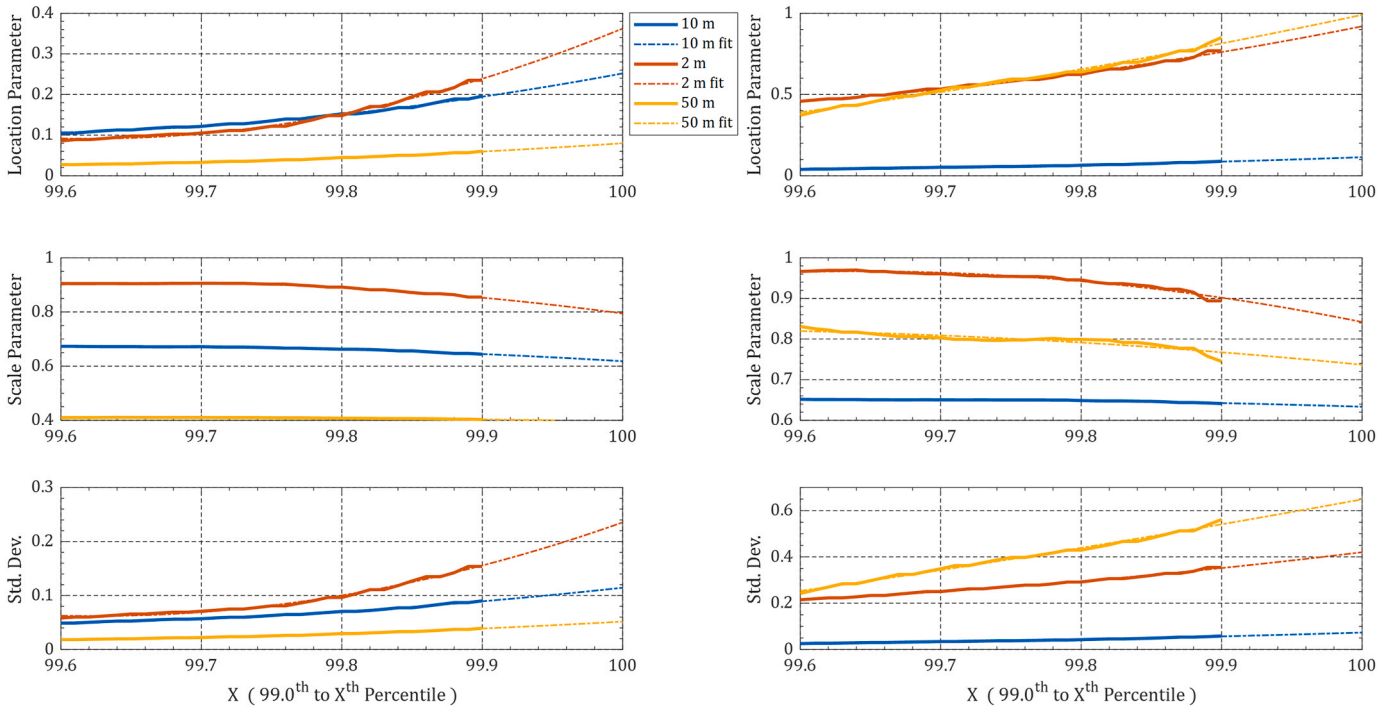

Fig. 20. The variation of scale and location parameters along with the standard deviation near the quantile (99. 0^{th} to 99.90th) to extrapolate curve the distribution parameters using a least squared error quadratic for the quantile (99. 0^{th} to 100^{th}). Plots in the left column correspond to station 44029 and that in the right column, station 44030.

Table 7
Correlation of the second-degree polynomial curve used to extrapolate the location parameter (C_{lo}), scale parameter (C_{sc}), and standard deviation (C_{sd}) for two stations 44029 and 44030 at the three depths given in percentage. The depth is in meters.

Station	Depth	C_{sc}	C_{lo}	C_{sd}
44029	2	99.71	99.41	99.79
44029	10	99.80	99.49	99.65
44029	50	99.86	99.36	99.87
44030	2	99.71	98.03	99.68
44030	10	99.64	97.14	99.76
44030	50	99.52	90.13	99.67

step in designing a continuous mussel dropper system for operation in U. S. Federal waters. We began by identifying a potential farm location based on specific criteria, including water depth, federal water boundaries, seafloor suitability for anchor piles, farm size, and proximity to coastal ports, using bathymetric and sedimentary maps. Note that while surficial geology maps are a good start in the marine spatial planning process, more site-specific, geotechnical data are needed for proper engineering analysis of anchors. The research then focused on modeling extreme environmental conditions at the chosen farm site. We developed a statistical model using historical annual maximum data from five wave monitoring stations and two current velocity stations in the New England region as waves and currents pose the primary threats to offshore mussel farming. We used the Weibull distribution to model extreme wave conditions and the largest 0.3 % data for extreme currents. This analysis provided insights into wave height, period, and wavelength for various return periods.

We also introduced an innovative method to analyze current profiles, improving precision. This new approach combines Spalding's wall function with a fourth-order polynomial framework. The resulting data served as crucial input for numerical simulations presented in the companion paper part II, guided by the Ultimate Limit State (ULS) criteria to ensure the structural integrity of mussel farm components.

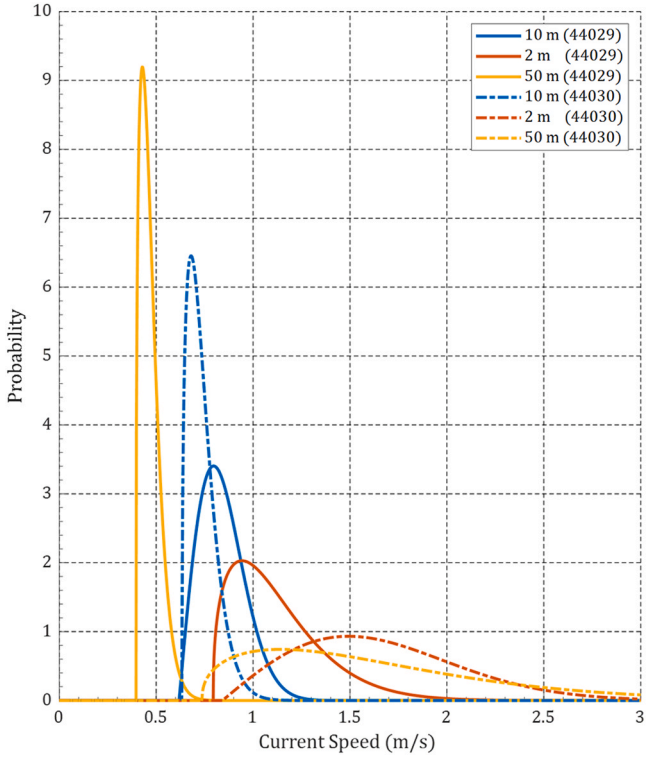

Fig. 21. The probability density functions for the two stations 44029 and 44030 at three water depths of 2 m, 10 m, and 50 m. Fitted models utilize 99. 0^{th} to 99. 9^{th} percentile data to model the return values. It uses extrapolated distribution parameters to account for the omitted data between the 99. 9^{th} 100^{th} percentile.

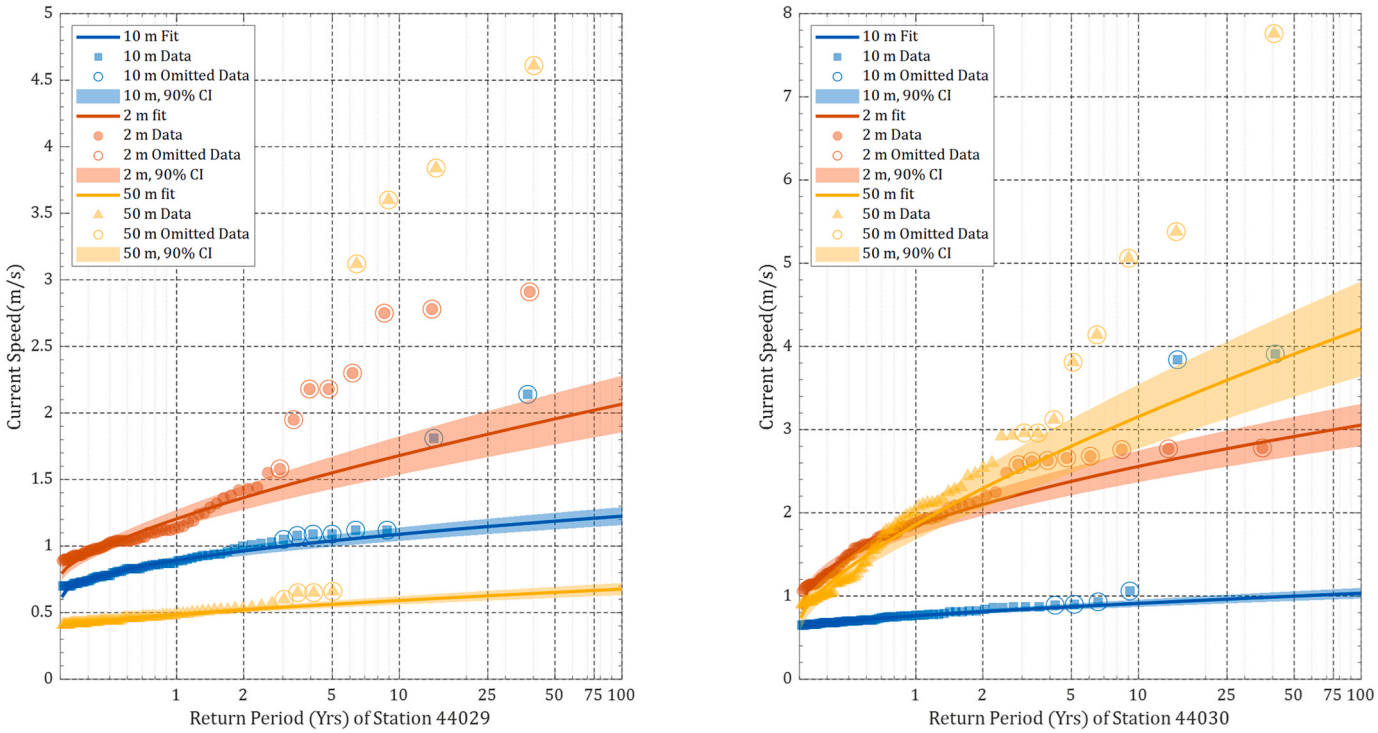

Fig. 22. Estimated return values for the current speeds for two stations 44029 and 44030 at depths of 2 m, 10 m, and 50 m. Fitted models utilize 99. 0^{th} to 99. 9^{th} percentile data to model the return values. It uses extrapolated distribution parameters to account for the omitted data between the 99. 9^{th} and 100^{th} percentile.

Table 8
Final return periods and return values for current speeds (m/s) at three different depths with 90 % CI for station 44029 estimated for the quantile (99.00^{th} – 100^{th}) representing the extreme events.

			Return Period			
	Depth (m)	Metric	10 Yr (m/s)	25 Yr (m/s)	50 Yr (m/s)	100 Yr (m/s)
Site 44029	2 m	Lik	1.6803	1.8407	1.9557	2.0663
	2 m	Max	1.8242	2.0129	2.1484	2.2789
	2 m	Min	1.5363	1.6684	1.7629	1.8537
	10 m	Lik	1.0889	1.1471	1.1871	1.2246
	10 m	Max	1.1393	1.2045	1.2495	1.2916
	10 m	Min	1.0385	1.0897	1.1248	1.1576
	50 m	Lik	0.5914	0.6268	0.6522	0.6766
	50 m	Max	0.6223	0.6638	0.6936	0.7223
	50 m	Min	0.5605	0.5898	0.6107	0.6309

Table 9
Environmental load conditions corresponding to the 10, 25, 50, and 100 yr return periods for the selected location with the most likely scenario and maximum within the 90 % CI. Here U stands for the current speed and ML stands for most likely. This study, suggests and uses (Part II) the use of ML values for the Hs and Max values for U as the U values are based on a single location (spatial variability) and the omitted outliers fall mostly above the max values.

Return Period	ML H_s (m)	Max H_s (m)	T_s(s)	Max U 1.38 m (m/s)	Max U 6.92 m (m/s)	Max U 34.61 m (m/s)
10 yr	8.03	10.12	11.87	1.824	1.139	0.6223
25 yr	8.85	11.02	12.21	2.013	1.205	0.664
50 yr	9.41	11.68	12.45	2.148	1.250	0.693
100 yr	9.93	12.20	12.63	2.279	1.292	0.722

Finally, we developed a joint probability density function, considering wave height and current velocity at a specific depth, assuming statistical independence. This model will be used in the companion paper, where we will estimate failure probabilities for mussel farm components. This research quantifying the extreme wave and current conditions in the offshore waters of New England contributes not only to advancing offshore mussel farming but also to all types of offshore aquaculture systems.

While this study aimed to conduct a comprehensive analysis of the extreme environmental conditions in New England's offshore waters, several limitations should be acknowledged. First, the potential farm location was defined based on bathymetric and surficial geology maps. Although these maps are useful for initial spatial planning, they are insufficient for detailed site selection. Site-specific geotechnical data analyses and considerations of navigational routes, protected zones for endangered species, and other regulatory constraints are necessary. Detailed geotechnical investigations are essential for proper engineering analysis of anchors, as they provide critical information about seafloor properties that cannot be inferred from surface maps alone. Second, the statistical modeling of extreme environmental conditions relied on historical annual maximum data from a limited number of wave and current monitoring stations. This approach may not fully capture the spatial variability and localized extreme events in the region, potentially affecting the accuracy of the extreme value analysis. The statistical models come with assumptions; for instance, they assume time independence, which may not effectively account for real physical phenomena such as climate change. While the Weibull distribution was used in this study, other distributions like the Gumbel distribution could also be applied and might yield different estimates of extreme loading conditions. Furthermore, the assumption of statistical independence in developing the joint probability density function for wave height and current velocity may oversimplify the complex interactions between these environmental factors, potentially leading to variations in the system response. In this study, a 50-year wave event is characterized by only two parameters: the significant wave height of the peak hour of the event and the corresponding wave period. However, different wave environments can have the same Hs (significant wave height) and Tp (peak period) values but create different responses in the system. Therefore, options such as loading the system with random waves based

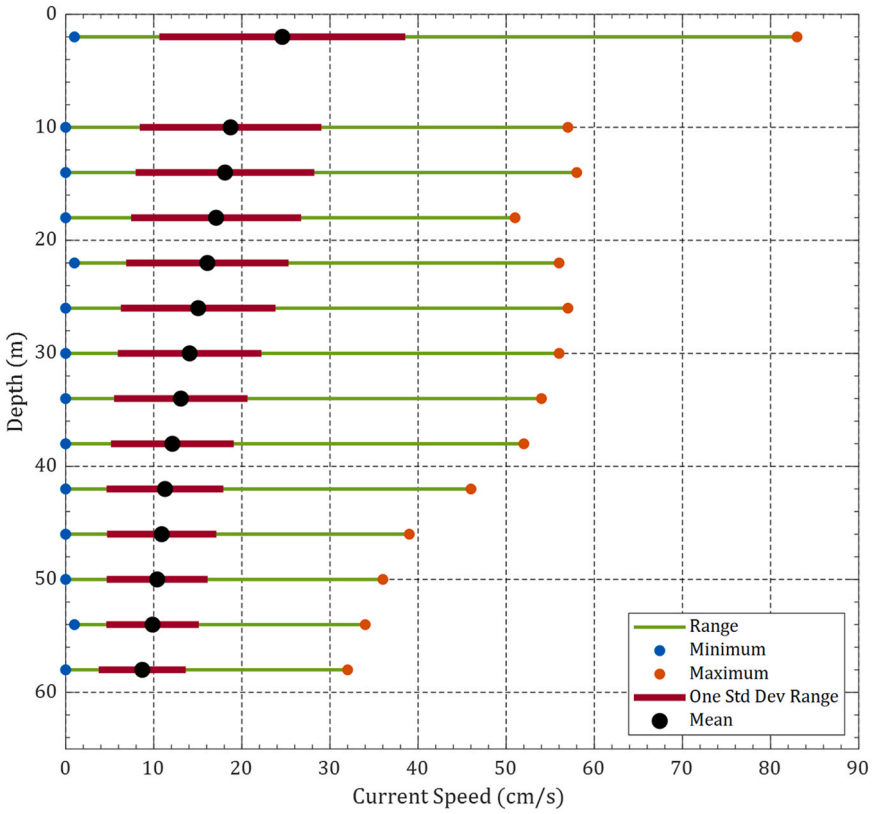

Fig. 23. Current speed profile from 45 days of hourly averaged data at station 44029. The profile consists of 14 depths and minimum (blue), maximum (orange), and mean (black) values are plotted along with one standard deviation range from the mean. The variation of profile shape for mean-one std, mean, mean+one std, and max, can be noted suggesting the need for different profile shapes depending on the quantiles.

on a wave spectrum model fitted for the Northeast region's extreme events should be considered in the future. Additionally, the random waves and currents are not unidirectional and are defined by the directional spectrum. This might not be crucial while the maximum stress is the only concern, however this is important for optimizing the system. Typical environmental conditions also play a crucial role in the design of offshore farms, as fatigue from cyclical loading is correlated with the number of cycles. While the newly proposed method of combining Spalding's wall function with a fourth-order polynomial enhances the analysis of current profiles, it requires further validation through field measurements. Moreover, the directional variation of the current along the depth was not modeled in this study. The numerical simulations presented are guided by the Ultimate Limit State (ULS) criteria, which test combinations of 50-year wave and 10-year current events. However, the possibility of more extreme events, such as the simultaneous occurrence of 50-year wave and 50-year current conditions, was not explored. Future research should address these limitations by incorporating site-specific geotechnical surveys, expanding the statistical models to include other distributions and dependencies between variables, considering directional variations of waves and currents, and validating numerical models with field data. This would enhance the accuracy of environmental condition assessments and improve the reliability of offshore mussel farm designs.

Note I: To clarify our buoy station selection and their representativeness of local hydrological conditions, we have included two figures in the Appendix (Figs. 29 and 30). Fig. 29 shows all nine NDBC stations within our defined region of interest, spanning the coastal area from north of Cape Cod, Boston, to approximately Portland, Maine. Of these, only six buoys have sufficient historical significant wave height data suitable for extreme value analysis; specifically, IOSN3 lacks wave height data, and buoys 44073 and CMLN3 have only five annual maxima data points each. We selected five buoys with reliable and extensive data records (20–40 years) for our analysis. Fig. 30 displays additional buoys outside our study region; incorporating these would require expanding the study area beyond our scope. For current speed data, only two buoys (stations 44029 and 44030) within our region have adequate historical records, and we included both. The only omitted buoy with wave data in the region of interest, station 44018, is the farthest from the farm site and less representative of local conditions. While including more monitoring points could enhance data comprehensiveness, our focus is on the defined region, and the selected buoys adequately represent the extreme environmental conditions relevant to the mussel farm site.

Note II: The title and authors of the companion paper (Part II) under review are given in Sunny et al. (2023).

Authorship statement

All persons who meet authorship criteria are listed as authors, and all authors certify that they have participated sufficiently in the work to take public responsibility for the content, including participation in the

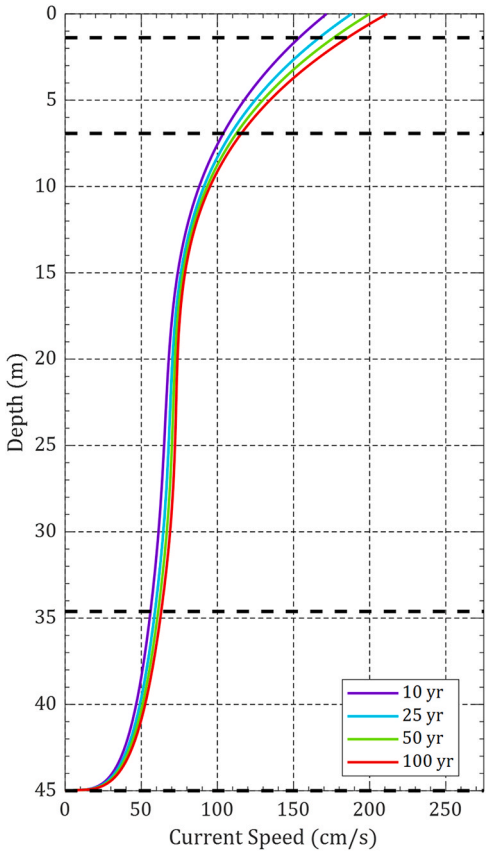

Fig. 24. Final current profiles for extreme current events at the design depth estimated. The current profile is interpolated using the newly proposed function that combines Spalding's wall function and fourth-order polynomial function. This profile represents the most likely velocity profiles for the extreme events at the selected location.

concept, design, analysis, writing, or revision of the manuscript. Furthermore, each author certifies that this material or similar material has not been and will not be submitted to or published in any other publication before its appearance in the Aquaculture Engineering (Elsevier).

CRediT authorship contribution statement

Bill Silkes: Writing – review & editing, Resources, Data curation. **Richards C. Sunny:** Writing – original draft, Visualization, Validation, Software, Resources, Methodology, Investigation, Formal analysis, Data curation, Conceptualization. **Longhuan Zhu:** Writing – review & editing. **Matthew Bowden:** Writing – review & editing, Supervision, Project administration, Funding acquisition. **David W. Fredriksson:** Writing – review & editing, Supervision, Resources, Project administration, Methodology, Funding acquisition. **Igor Tsukrov:** Writing – review & editing, Supervision, Software, Resources, Investigation. **Michael Chambers:** Writing – review & editing, Supervision.

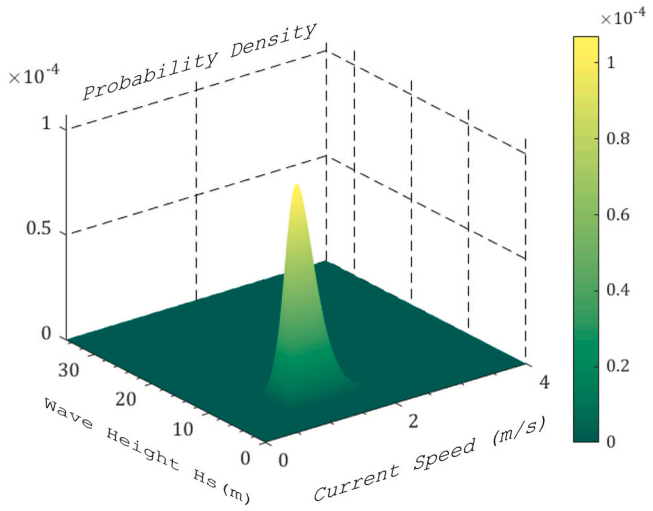

Fig. 25. This figure presents the joint probability density function (JPDF) combining the PDFs of annual maxima wave heights and extreme current speeds. The JPDF illustrates the combined variability between these two environmental parameters, providing insights into their concurrent distribution. The elevated peak indicates the most likely combinations of the annual maximum wave height and current speed, which are crucial for understanding the coupled dynamics of wave-current interactions and risk assessment for offshore structures. The single localized peak with rapidly reducing likelihoods away from the peak suggests extreme events with wave heights larger than 12 m and current speeds more than 3 m/s are very less likely. It can be also referenced that the likelihood of annual maximum Hs to be less than 4 m and the annual maxima current speed less than 0.5 m/s is very low.

Declaration of Competing Interest

The authors declare that they have no known competing financial interests or personal relationships that could have appeared to influence the work reported in this paper.

Data availability

Data will be made available on request.

Acknowledgement

We gratefully acknowledge the funding and support provided by the National Marine Fisheries Service (NMFSC), Office of Aquaculture for this project. We also extend our appreciation to the anonymous reviewers from NOAA for their reviews and feedback. Additionally, we thank Tobias Dewhurst, Zachry Devonski, Corey Sullivan, Zach Moscicki, and Zachary Gordon for their valuable comments that contributed to the refinement of this work. I have utilized ChatGPT and Grammarly to improve the readability and clarity of some sentences in this manuscript. Both tools were employed to assist in refining language and grammar, but they did not contribute to the technical or scientific content of the paper.

Appendix A. Appendix

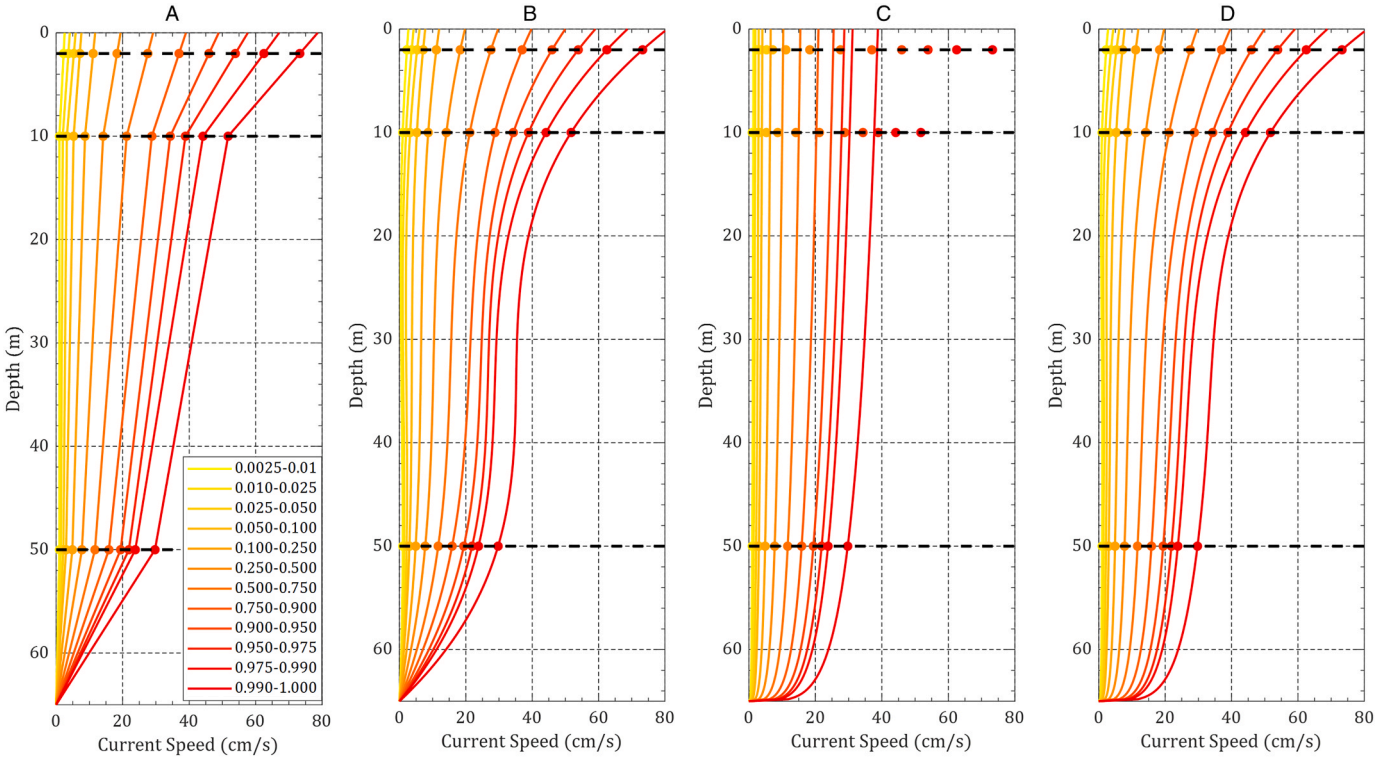

Fig. 26. Current speed quantile profiles to represent the 45 days of station 44029 data created using the piecewise linear, cubic, Spalding's wall function, and a newly proposed function. Profiles are created using data at the three depths which are available for the historical data; i.e. 2, 10, and 50 m. A) Piecewise linear fit, B) Cubic polynomial C) Spalding's wall function, D) New proposed function. Dots are the measured data points.

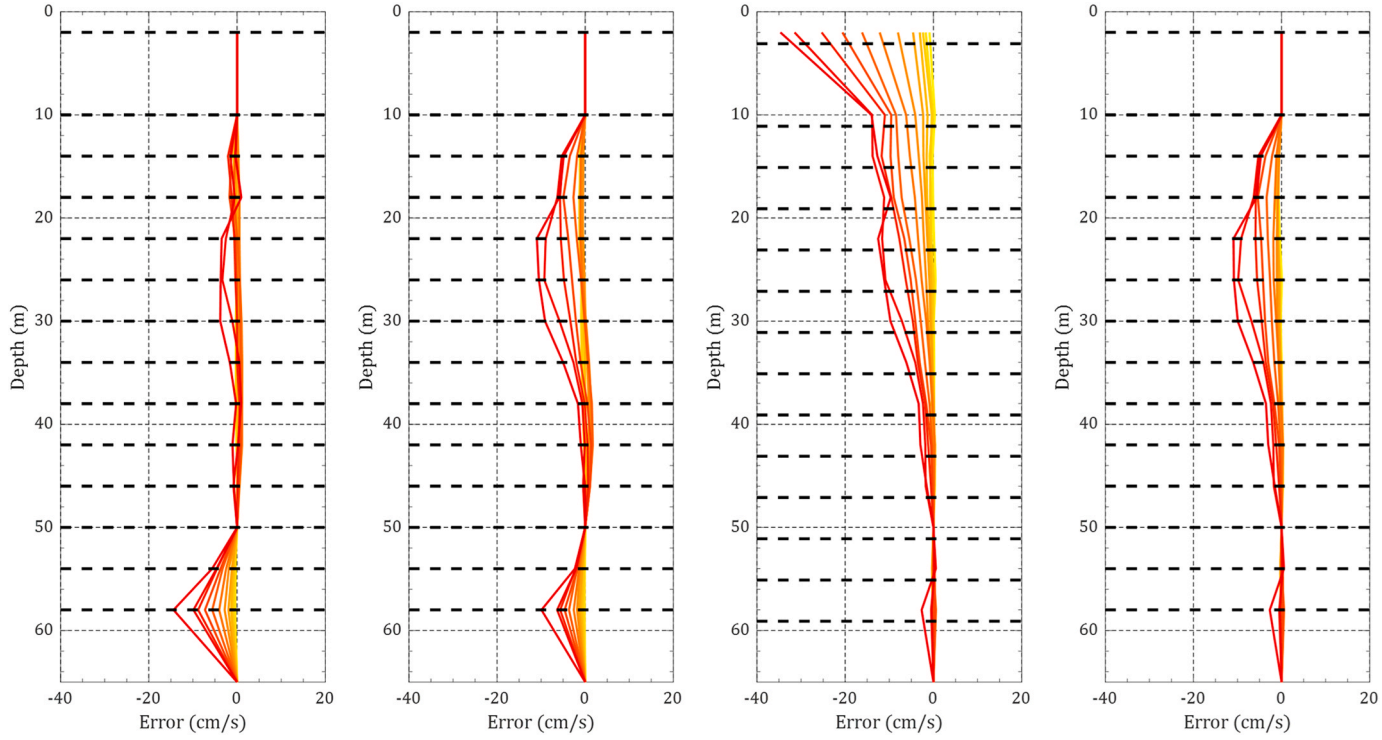

Fig. 27. Errors associated with the current speed profiles created using four functions at 14 depths. A) Piecewise linear fit, B) Cubic polynomial C) Spalding's wall function, D) New proposed function.

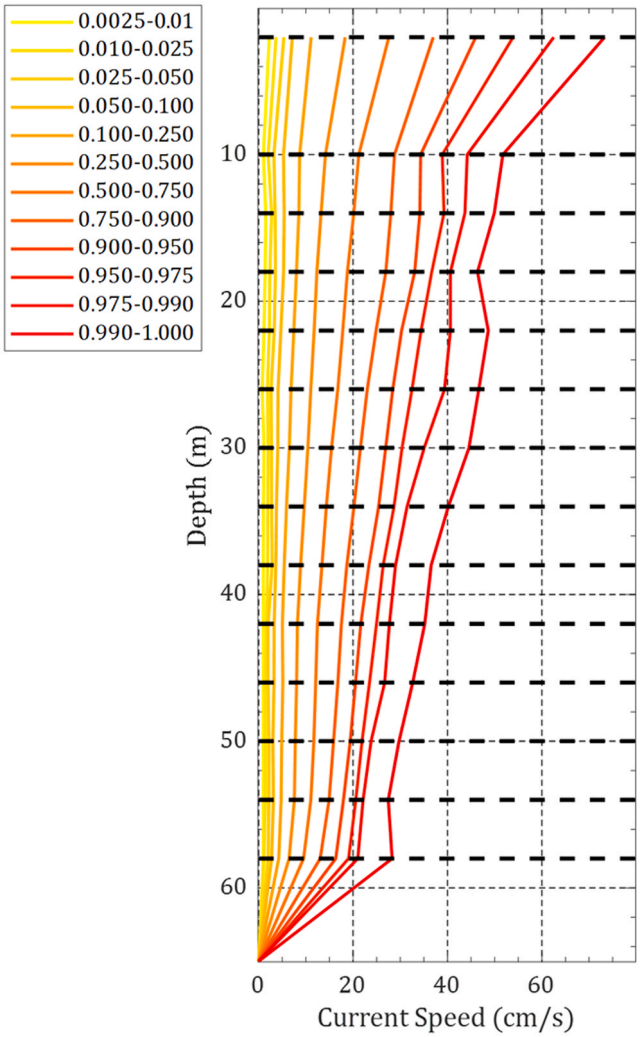

Fig. 28. Piecewise linearly fit Quantile mean current profiles of 45 days of hourly averaged data at station 44029.

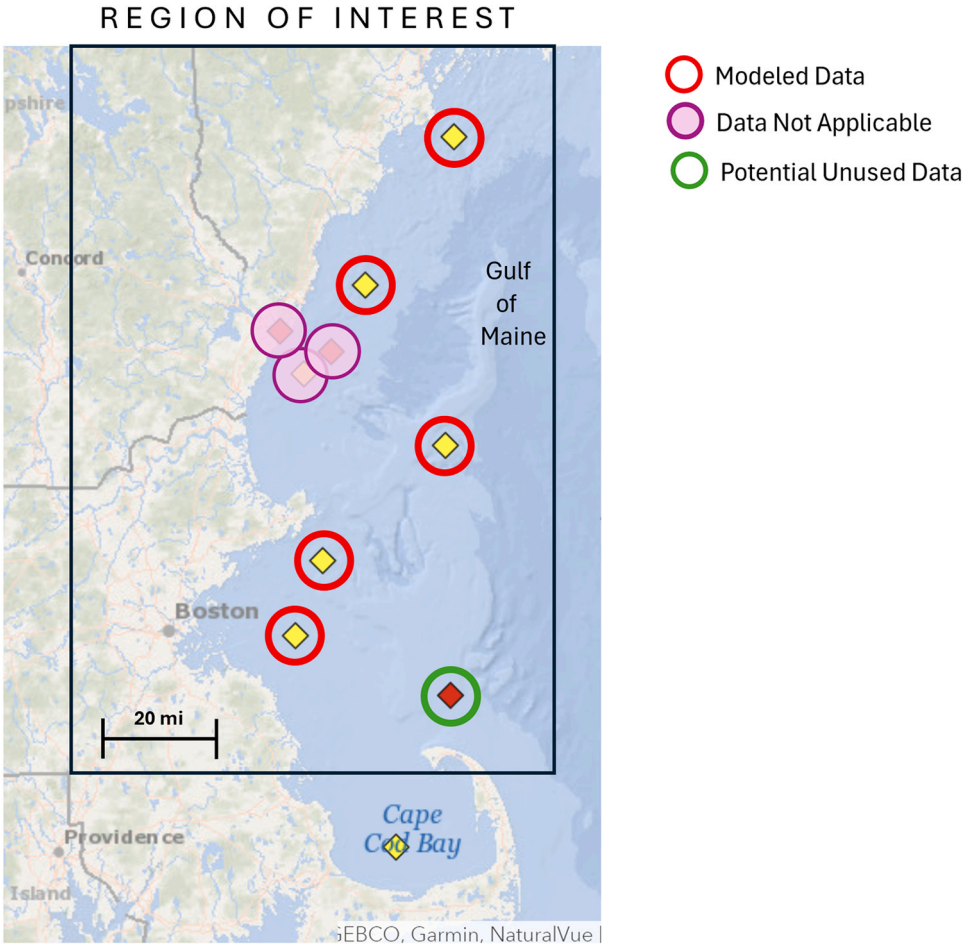

Fig. 29. Map of the region of interest showing buoy stations in the New England offshore waters from the NDBC website. The map displays all nine National Data Buoy Center (NDBC) stations within this region. Buoys with sufficient historical significant wave height data used in our analysis are highlighted. These selected buoys provide reliable and extensive data records (20–40 years) essential for modeling extreme environmental conditions relevant to the potential mussel farm site. Buoys without adequate data or those located farther from the farm site are also indicated.

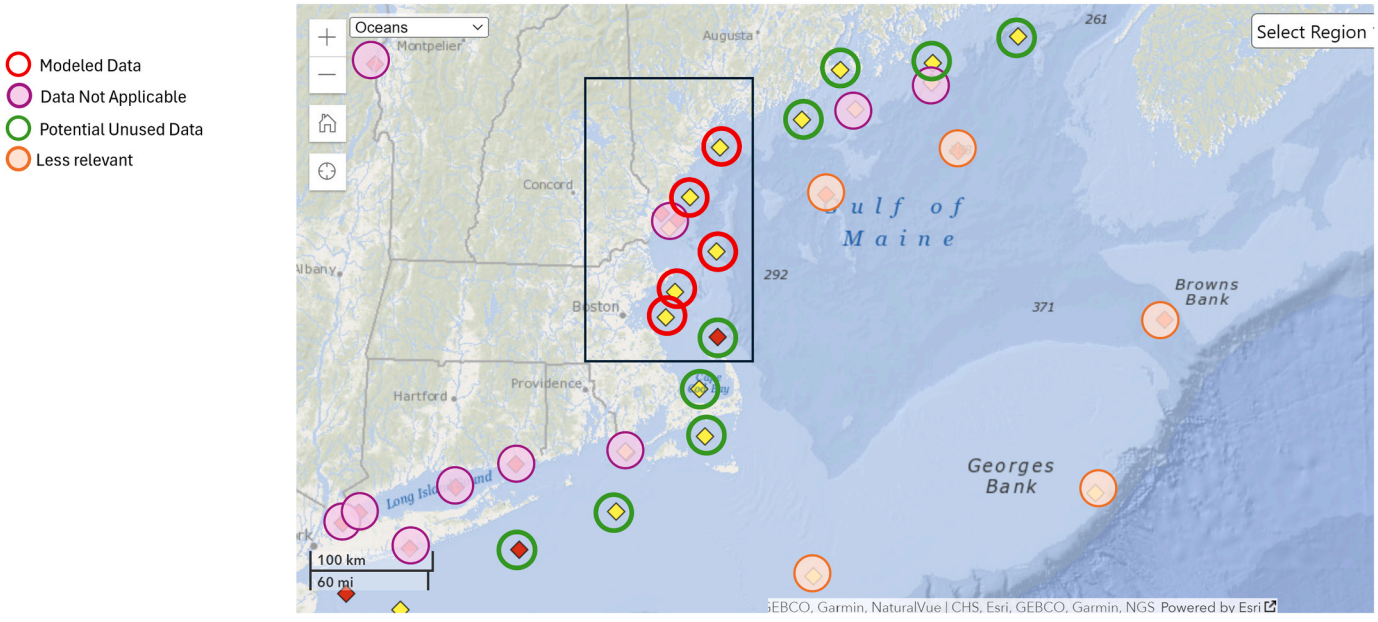

Fig. 30. National Data Buoy Center (NDBC) and Integrated Ocean Observing System (IOOS) stations located inside and outside the defined rectangular region of interest. The buoys outside the region of interest were not included in the analysis as they are less representative of the local hydrological conditions at the proposed mussel farm site. Incorporating these stations would help to study the entire northeast offshore region viable for aquaculture, but it requires expanding the study area, which was beyond the scope of this work.

References

Blumberg, A.F., Mellor, G.L., 1987. A description of a three-dimensional coastal ocean circulation model. Three-Dimens. Coast. Ocean Models 4, 1–16.

Cartwright, D., Edden, A.C., 1973. Corrected tables of tidal harmonics. Geophys. J. Int. 33, 253–264.

Cole, R., 2002.Impacts of marine farming on wild fish populations. report for new zealand ministry of fisheries, national institute of water and atmospheric research, auckland, new zealand.

Dean, R.G., Dalrymple, R.A., 1995. Water wave mechanics for engineers and scientists. World Scientific.

Flagg, C.N., Kim, H.S., 1998. Upper ocean currents in the northern arabian sea from shipboard adcp measurements collected during the 1994–1996 us jgofs and onr programs. Deep Sea Res. Part II: Top. Stud. Oceanogr. 45, 1917–1959.

Goda, Y., 2010. Random seas and design of maritime structures. World Scientific. https://doi.org/10.1142/7425.

Goodman, T.R., Breslin, J.P., 1976. Statics and dynamics of anchoring cables in waves. J. Hydronautics 10, 113–120.

Gorelick, N., Hancher, M., Dixon, M., Ilyushchenko, S., Thau, D., Moore, R., 2017. Google earth engine: planetary-scale geospatial analysis for everyone. Remote Sens. Environ. 202, 18–27.

Grizzle, R.E., Malik, M.A., Ward, L.G., 2009.High-resolution seafloor mapping and an assessment of the effectiveness of the western gulf of maine closure area (wgomca). Workshop on Integrating Seafloor Mapping and an Assessment of the Effectiveness of the Western Gulf of Maine.

Haidvogel, D.B., Arango, H.G., Hedstrom, K., Beckmann, A., Malanotte-Rizzoli, P., Shchepetkin, A.F., 2000. Model evaluation experiments in the north atlantic basin: simulations in nonlinear terrain-following coordinates. Dyn. atmospheres Oceans 32, 239–281.

Hall, S.G., Campbell, M., Geddie, A., Thomas, M., Paul, D., Wilcox, D., Smith, R., Eddy, N., Frinsko, M., Wilder, S., et al., 2018.Engineering challenges in marine aquaculture, In: 2018 ASABE Annual International Meeting, American Society of Agricultural and Biological Engineers.1.

Hsu, T.W., Ou, S.H., Liau, J.M., 2005. Hindcasting nearshore wind waves using a fem code for swan. Coast. Eng. 52, 177–195.

Kadivar, M., Tormey, D., McGranaghan, G., 2021. A review on turbulent flow over rough surfaces: fundamentals and theories. Int. J. Thermofluids 10, 100077.

Kurt Menke, G., Smith Jr, R., Pirelli, L., John Van Hoesen, G., et al., 2016. Mastering QGIS. Packt Publishing Ltd.

Landmann, J., Ongsiek, T., Goseberg, N., Heasman, K., Buck, B.H., Paffenholz, J.A., Hildebrandt, A., 2019. Physical modelling of blue mussel dropper lines for the development of surrogates and hydrodynamic coefficients. J. Mar. Sci. Eng. 7, 65.

Lloyd, B.D., 2003.Potential effects of mussel farming on New Zealand's marine mammals and seabirds: a discussion paper.Department of Conservation.

Lynett, P.J., 2006. Nearshore wave modeling with high-order boussinesq-type equations. J. Waterw. Port. Coast. Ocean Eng. 132, 348–357.

Oke, P., Proctor, R., Rosebrock, U., Brinkman, R., Cahill, M., Coghlan, I., Divakaran, P., Freeman, J., Pattiaratchi, C., Roughan, M., et al., 2015. The marine virtual laboratory: enabling efficient ocean model configuration. Geosci. Model Dev. Discuss. 8, 9741–9768.

Sobey, R.J., 1992. A local fourier approximation method for irregular wave kinematics. Appl. Ocean Res. 14, 93–105.

Spalding, D.B., et al., 1961. A single formula for the law of the wall. J. Appl. Mech. 28, 455–458.

Sunny, R.C., Fredriksson, D.W., Tsukrov, I., Zhu, L., Bowden, M., Chambers, M., Coogan, M., Silkes, B., 2023.Design considerations for a continuous mussel farm in new england offshore waters. part ii: Using validated numerical models to estimate the probability of failure.Under Review.

Tayfun, M.A., 1980. Narrow-band nonlinear sea waves. J. Geophys. Res.: Oceans 85, 1548–1552.

Troell, M., Naylor, R.L., Metian, M., Beveridge, M., Tyedmers, P.H., Folke, C., Arrow, K. J., Barrett, S., Crépin, A.S., Ehrlich, P.R., et al., 2014. Does aquaculture add resilience to the global food system? Proc. Natl. Acad. Sci. 111, 13257–13263.

I.W. Wieling, 2023.Recommended design practice for offshore and nearshore seaweed growing systems, version 1.0 2023. (https://northseafarmers.org/projects/20230330_recommended_design_practice_v1.0_signed.pdf).[Accessed 12-Oct-2023].